Int J Earth Sci (Geol Rundsch) (2013) 102:875–901
DOI 10.1007/s00531-012-0829-5

ORIGINAL PAPER

Identification of maars and similar volcanic landforms in the West Eifel Volcanic Field through image processing of DTM data: efficiency of different methods depending on preservation state

Nadine Seib · Jonas Kley · Georg Büchel

Received: 11 January 2012 / Accepted: 30 September 2012 / Published online: 21 November 2012

Abstract The West Eifel Volcanic Field comprises 98 maars, tuff rings, and scoria rings of volcanoes younger than 700 ka. Digital Terrain Models (DTMs) allow to automatically measure morphologic parameters of volcanic edifices such as slope angles, diameters, elevations, floor, and slope surface areas. Based on their morphological characteristics, we subdivided the West Eifel volcanoes into five morphometric groups which reflect different stages of erosion. Group I, II, and IV comprise clear ring-shaped structures. The difference between these groups is that a tephra ring is well preserved in Group I, partially preserved in Group II and absent in Group IV. The original shapes of Group III maars have been lost more substantially than in Groups I, II, or IV, but they nevertheless retain a negative shape (a depression) and have characteristic channel systems, which can be used as search criteria. Maar-diatremes of Group V are eroded down to their feeder pipes and form hills. In order to locate potential volcanic depressions that are likely to be maar volcanoes, we defined common search criteria such as circular negative landforms or particular drainage system patterns for all groups except the least well-preserved Group V. These criteria were taken as the basis for further processing of the DTM data. The first processing step consisted of constructing a residual relief calculated as the difference between a filtered (smoothed) topographic surface and the original DTM data. This identifies local topographic features. We propose a method for regulating the degree of smoothing which is based on filtering of local maxima according to their distance from a surface constructed from local minima. The previously defined search criteria for Groups I to IV such as specific ranges of curvature, slope, circularity, density of the drainage network were then applied to the residual relief in order to extract maar shapes. Not all criteria work equally well for all morphological groups. Combinations of multiple search criteria therefore yield the best results and efficiently identify most known maars. They also separate some probable new, hitherto unrecognized maars from a large number of other local depressions. We also compared the erosional state of maars to their absolute ages. Published estimates of erosion rates for maars in the French Massif Central suggest a general trend of erosion rates decreasing with time elapsed since eruption. However, this cannot explain the strongly varying ages for maars of the same morphometric group (i.e., similar preservation state) in the West Eifel Volcanic Field. The spatial distribution of the morphometric groups shows some regularity. For example, strongly eroded maars are concentrated in the Gerolstein area (where maar density is highest), whereas most well-preserved maars are located east of the Eifel North–South Depression (ENSD). Most maars affected by fluvial erosion lie near the Kyll and Kleine Kyll streams. These observations suggest differential recent uplift of the West Eifel Volcanic Field, with stronger uplift occurring west of the ENSD.

N. Seib (✉) · G. Büchel
Institut für Geowissenschaften, Fredrich-Schiller-Universität Jena, Burgweg 11, 07749 Jena, Germany
e-mail: nadine.seib@uni-jena.de

G. Büchel
e-mail: georg.buechel@uni-jena.de

N. Seib
Institut für Geowissenschaften, Technische Universität Bergakademie Freiberg, Bernhard-von-Cottastr. 2, 09596 Freiberg, Germany

J. Kley
Geowissenschaftliches Zentrum, Georg-August-Universität Göttingen, Goldschmidtstr. 3, 37077 Göttingen, Germany
e-mail: jonas.kley@geo.uni-goettingen.de

Keywords Volcanoes · Maar · Crater · Tuff ring · Remote sensing · Geomorphology · GIS · DTM · Erosion rate · Surface reconstruction · Eifel north–south zone

Introduction

Maar volcanoes of Cenozoic age are the dominant geological features of the Eifel region (Figs. 1, 2, 5). They also form a main touristic attraction (Schmincke 2007). Present volcanic activities are limited processes reflected by mineral and thermal springs, CO_2 outgassing (May et al. 1996; May 2005; Schmincke 2010) and uplift (Illies et al. 1979; Garcia-Castellanos et al. 2000; Meyer and Stets 2002; Schäfer et al. 2005).

The Cenozoic volcanoes were emplaced on a substratum of deformed Paleozoic rocks (Fig. 1). Folds and thrust faults of Variscan (Late Carboniferous) age are reflected in the NE–SW orientation of some major valleys. After the Late Paleozoic, a peneplain formed on the Rhenish Massif which was partly covered by Mesozoic sediments (Ziegler and Dèzes 2007). In Cenozoic time, uplift and incision have shaped the Rhenish Massif. Mertes (1983) pointed out that the West Eifel Volcanic Field is cross-cut by the eastern edge of the Eifel North–South Depression (ENSD). This is a large-scale linear structural low outlined by the occurrence of Triassic strata and aligned axial depressions of the Variscan folds. It extends from southern France through Luxembourg into the Eifel region and is assumed to have been active since Devonian time by some authors (Garcia-Castellanos et al. 2000; Meyer and Stets 2002; Shaw et al. 2005; Schäfer et al. 2005).

The Cenozoic volcanism of the Rhenish Massif occurred in two main stages: the first in the Eocene to Miocene [40–20 Ma (Lustrino and Carminati 2007), 45–24 Ma (Wilson and Downes 1991; Ziegler and Dèzes 2007), 44–35 Ma (Fekiacova et al. 2007)] and the second one in Quaternary time [0.9 Ma–9 ka (Schmincke 2007; Büchel 1993, 1994)]. Traces of volcanic landforms in various stages of degradation stand out in the present-day landscape.

The older, Tertiary eruption centers are strongly eroded, often down to their root zones where only narrow basaltic necks or dykes have remained of the volcanic edifice (Büchel 1992). In the area of the Kelberg (Fig. 2), a prominent regional magnetic anomaly, relatively large

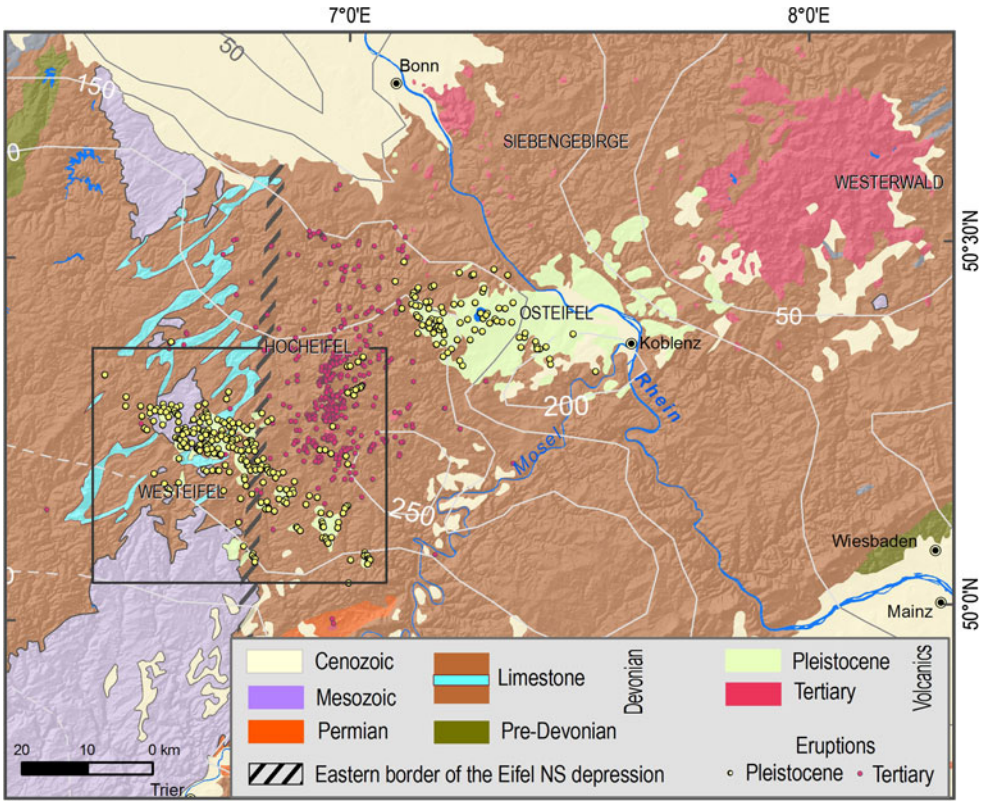

Fig. 1 Location of the western Eifel volcanic field within the Variscan Rhenish Massif. *Shaded* SRTM 90 elevation data overlaid with geological map (modified from digital geological map; Bundesanstalt für Geowissenschaften und Rohstoffe, 2003). Eruption centers of the Westeifel Volcanic Field after Büchel and Mertes (1982); eruption centers of the Hocheifel Volcanic Field after Huckenholz and Büchel (1988); eruption centers of the Osteifel Volcanic Field after Viereck (1984). White contour lines denote uplift of the Rhenish Massif (in m) during the last 800,000 years (Schäfer et al. 2005). Source of the SRTM data: http://srtm.csi.cgiar.org

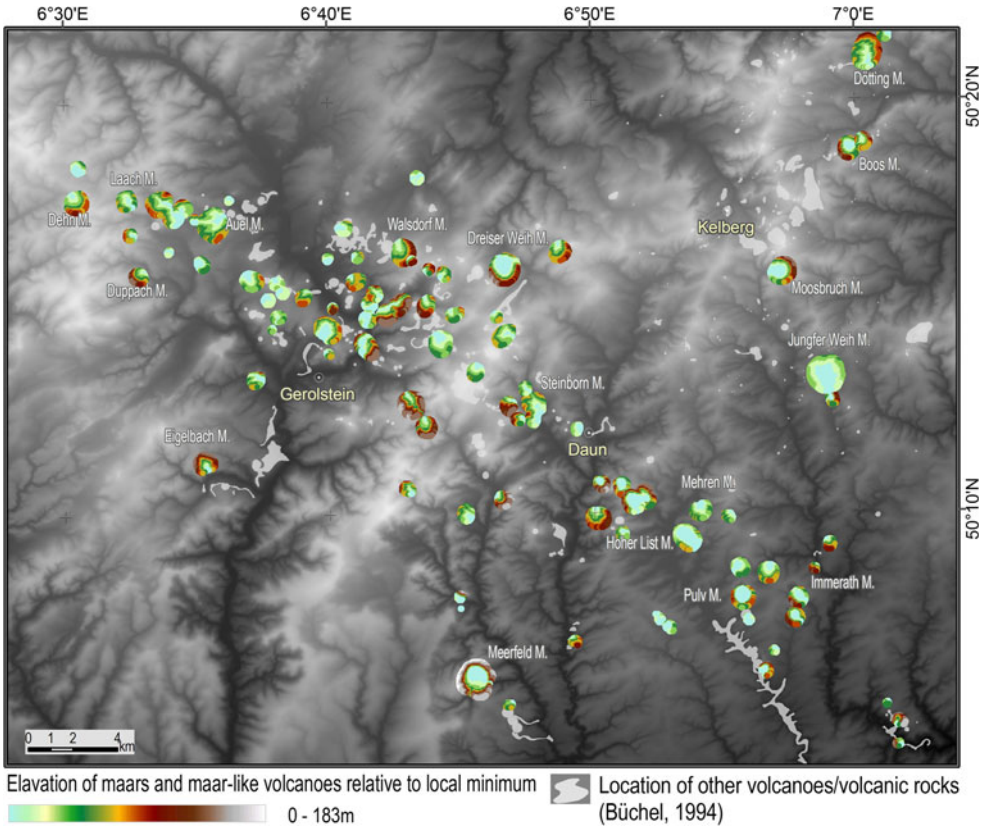

Fig. 2 Location of the Westeifel volcanoes. Background is DTM (Digital Terrain Model) data. For maars, tuff rings, and scoria rings, the relative elevations above the crater floors are shown by *color coding*

fields of Tertiary tuff diatremes and intrusions are found (Büchel 1994). Most remains of Tertiary volcanoes constitute positive landforms (hills) and were recognized and mapped in the field.

The onset of Quaternary volcanism in the West Eifel Volcanic Field coincides with beginning uplift of the Rhenish Massif (Mertes and Schmincke 1985; Ziegler and Dèzes 2007). Based on paleomagnetic measurements, the youngest Main Terrace is inferred to be slightly younger than the Brunhes-Matuyama magnetic epoch boundary, that is, 0.78–0.8 Ma (Garcia-Castellanos et al. 2000; Meyer and Stets 2002; Schäfer et al. 2005; Ziegler and Dèzes 2007). Several authors have pointed out the link between Quaternary volcanism and uplift of the area.

During the last 0.8 Ma, the Rhenish Massif has risen by 200–250 m (Meyer and Stets 2002; Garcia-Castellanos et al. 2000; Schäfer et al. 2005). This has led to increased fluvial incision and erosion (Büchel 1987), largely obliterating the original form of some eruption centers and making their recognition difficult.

So far, 257 eruption centers of Quaternary age have been ascertained in the West Eifel Volcanic Field, and 19 more are assumed but remain to be confirmed (unpublished own data). Their ages range from 0.9 Ma to 9 ka (Meyer and Stets 2002; Schmincke 2007, Büchel 1994). Different methods of dating such as $^{40}Ar/^{39}Ar$, K/Ar, ^{14}C and pollen analyses have been used to determine the age of explosions. 66 % of the volcanoes are scoria cones of which 53 % have associated lava flows. The scoria cones are on average 40 m (max. 100 m) high and 430 m (max. 600 m) in diameter (Büchel and Mertes 1982). In most cases, they are easily recognizable and can be mapped in the field or from remote sensing data without special processing. Due to this, scoria cones are not further treated here.

Of the known Quaternary volcanoes, 98 are maars or similar forms such as tuff rings and "scoria rings". Tuff rings, like maars, comprise broad and relatively thin deposits of ejecta, but their craters do not cut below the original ground surface (White and Ross 2011). Scoria cones, as the name implies, are volcanoes that have cone-like shapes and thick near-vent deposits that thin very rapidly outward (White and Ross 2011). Scoria volcanoes with large craters have been called scoria rings by some researchers (e.g., Büchel 1994). They cannot be distinguished from maars by the analysis of landforms alone. All these types constitute circular structures with diameters between 100 and 1,600 m. Several maars stand out in the present-day relief. The most recent ones have a nearly pristine form with a well-preserved rim and crater (Fig. 2). Others, however, are strongly eroded despite their young age. They are preserved as relics or entirely covered. This is why some maars were only discovered using gravity

(Büchel and Pirrung 1993; Stachel and Büchel 1989) and magnetic measurements (Lorenz and Büchel 1980).

In an earlier paper (Seib et al. 2008), we have processed DTM data to reveal subdued maar-shaped landforms which probably, and in some cases demonstrably, represent additional, hitherto unrecognized volcanoes. However, some methods used yielded a very large number of indistinct circular shapes that could only be interpreted visually and subjectively. In the present work, we apply methods of statistical analysis to separate eroded and buried maars from other negative landforms and use quantitative characteristics to obtain more objective assessments. We analyze in detail the morphological features of known maar structures, enabling us to strongly narrow down our search criteria.

Morphological characteristics of maars

Originally, the term "maar" was coined to describe particular topographic features, that is, bowl-shaped craters encircled by a low rim (Büchel 1993). Büchel (1993) proposed to use the term for "the whole [volcanic] structure and its formation. [It]…comprises the ring (tephra below the tuff rim), the crater sediments, the diatreme, and the feeder dyke system". Since maars are the near-surface expression of diatremes or explosion pipes, the entire system is now sometimes denoted as a maar-diatreme volcano (Lorenz and Kurszlaukis 2007; White and Ross 2011). These volcanoes can be associated with different magma types, such as alkali basalts, lamproites, or kimberlites (Martin et al. 2007; White and Ross 2011). Maar-diatreme eruptions are episodic (White and Ross 2011). However, the manifestation of maar-diatreme volcanism is known in many parts of the planet: Africa (Franz et al. 1997; Garcin et al. 2006; Lorenz and Kurszlaukis 2007; Schmincke 2010); New Zealand (Németh 2001; Németh and White 2003b); Alaska (Pirrung et al. 2008; White and Ross 2011); Hungary (Németh et al. 2003); Argentina (Ross et al. 2010); the French Massif Central (Degeai 2004); Central Spain (Martín-Serrano et al. 2009); Canada (Smith and Berryman 2007); Siberia (Kamenetsky et al. 2004), and others. New research into maar-diatreme eruptions of the World indicates that maar volcanoes can develop in different geological and geographical settings (Martin et al. 2007).

Maar-diatreme volcanoes have downward-narrowing, carrot-shaped eruption channels. In the initial post-eruptive stage, maar craters are often occupied by lakes, resulting in partial filling by lake sediments (Lorenz 2003; Pirrung et al. 2008).

Today, there are two principal theories on the maar-diatreme-forming process. The phreatomagmatic theory (Lorenz 1973, 1975, 1986; Büchel 1994; Lorenz 2003; Schmincke 2007) explains the explosions as the result of rising melt interacting with groundwater. The gas–fluid theory (Sorohtin 1985; Sorohtin and Ushakov 2002; Walters et al. 2006; Wilson and Head 2007; Russell and Moss 2006; Moss et al. 2008; Cas et al. 2008) interprets the eruption to result from the fluid pressure in rapidly propagating, wedge-shaped fissures. At any rate, a characteristic of this kind of eruption is the high water content of the ejected material. The eruption builds a relatively low rim of loose, moist tephra which is prone to landsliding and rapid erosion (Lorenz 2003). Disrupted aquifers fill the maar crater with water, creating maar lakes. For instance, a shallow lake had formed during the weeks following the formation of the Ukinrek maar (Pirrung et al. 2008).

Typical sizes and morphological parameters of maars according to Lorenz (2003) are listed in Table 1.

Wood (1974) derived ratios of diameter over crater depth for Mexican maars. For young maars, he determined ratios between 5 and 6. Even though the Mexican maars are unusual for having formed in an arid to semi-arid climate, Büchel (1993) showed that these values also hold for some young Eifel maars. The older the maars are, the lower the

Table 1 Basic characteristics of maar-diatreme volcanoes

Morphological elements	Parameters
Diameter	From 100 to 2,000 m (up to 5,000 m according to Beget et al. 1995)
Crater depth	From a few dozens of m to 300 m
Tephra ring	From a few m to probably 100 m height (up to 200 m according to Németh 2001)
Slope of the inner crater rim	>33°
Slope of the outer rim	5°–10°
Cone-shaped rims	Rims are sloping on average 75°–85° toward the center (Lorenz 2007); 50°–60° inferred from geophysical data (Schulz et al. 2005)
Diatreme depth	From a few tens of m to 2.5 km (Lorenz 1986); an approximate theoretical diatreme depth H can be calculated from the crater radius R and the inclination of the diatreme boundary (α: $H = R \times \tan \alpha$; for $\alpha = 82°$ $H = 7.1R$; for $\alpha = 65°$, $H = 2.1R$)

ratio becomes and the more the crater depth decreases as a result of post-eruptive filling (Büchel 1993). Shortly after the explosion, tephra slides down from the inner crater rim and partially backfills the crater (Lorenz 2003; Németh and Cronin 2007; Pirrung et al. 2008). Some roofs may collapse if the actual weight of the tephra is too high or when the syndepositional or postdepositional (rain) moisture increases its weight beyond the roofs' static stability (Lorenz 2007). Schaber and Sirocko (2005) found a maximum sediment thickness in the crater of 1/20 to 1/11 the crater diameter.

We have recalculated the ratio between crater diameter and depth, assuming a maximum sediment thickness of 1/11 the diameter. For maars with a tuff ring, the mean of the recalculated ratios is 4.97 and the mode is 5.1. For maars with no tuff ring, the mean is 6 and the mode is 7 (Table 2). These results for the West Eifel Volcanic Field maars agree well with Mexican maars. Similar proportions were also measured for the Ukinrek maars of Alaska, created by eruptions in 1977. The respective values for these maars are: Ukinrek West, 168–97 m: 32 m = ~5.3–3; Ukinrek East, 307 m: 71 m = ~4.3 (Pirrung et al. 2008). However, these observations can only be applied to young maars. Suhr et al. (2006) describe long-term continuous subsidence of diatremes over tens of millions of years, most likely due to compaction of the crater fill. This is why thick sediment successions can accumulate in old maars (e.g., 120 m of sediments in the 44 Ma Eckfelder Maar; Pirrung et al. 2003).

The proportion of crater depth to diameter also changes over time. Erosional processes including landslides normally increase crater diameters and reduce crater depth with time. Accordingly, the ratio of crater diameter to crater height should increase with age (Büchel 1993; Németh and Cronin 2007; Ross et al. 2010).

The slope angles of maars strongly depend on the volume of ejected material and the pre-eruption topography (Büchel 1993), but also on the moistness of the tephra and erosion processes such as slope failure (Lorenz 2003, 2007). The original shape of maars can also be influenced by the explosion direction (Németh 2001).

Effects of erosion on the form of maars

Over time, the shape of many maars has been strongly modified by erosional processes, which in turn depend on climate, tectonic processes and the properties of the rocks constituting the maar. The erosion of the Eifel volcanoes and of the entire region has not been investigated in much detail. Some aspects of erosion were studied in other volcanic regions (see below), but the field of research is still evolving and presents many open questions.

Büchel (1993) and Németh (2001) described different erosional stages of maar volcanoes. Büchel (1993) discerned the following five stages:

(a) Initial stage.
(b) Lake stage.
(c) Filled stage.
(d) Moderately eroded stage (ring rim and crater sediments destroyed).
(e) Strongly eroded stage (only feeder pipe or "root" remains).

Németh (2001) proposed only three erosional stages:

1. Initial stage (positive land forms, several hundred meters wide, with lake sediments).
2. Moderately eroded (exhumed volcanic pipes filled with pyroclastic breccias).
3. Strongly eroded (only exhumed feeder pipe remains).

Erosion rates vary over these stages. The tuff rim consisting of volcanic ash and disintegrated country rock erodes faster than the intact country rock. The deposition of thick, coarse-grained tephra often brings about slope instability and failure, whereas ash deposits rarely show this effect (Schaber and Sirocko 2005). High water content of the tephra also promotes intense mass movements (Lorenz 2007). The strong relief of the pristine ring rim induces rapid erosion with rates decreasing as the relief decays. After destruction of the ring rim, erosion rates must drop. Although the poorly consolidated crater sediments are susceptible to rapid erosion, their position in depressions surrounded by Devonian rocks will shield them. This explains the long-term preservation of shallow, bowl-shaped maar remains, such as the Jungfernweiher Maar (130 ka) and Döttinger Maar (390 ka). When the rims of maars are incised by rivers, the crater sediments are rapidly removed and the crater deepens again (Geeser Maar).

Morphological classification of the Eifel maars

We analyzed the mapped maars of the Eifel field with regard to their morphological properties. Characteristic profiles are shown in Fig. 3 and elevation data in Table 1. Expanding the existing classification of erosional stages (see above), we subdivided them into five classes as follows (Figs. 3, 4):

I. Maars easily recognizable by the presence of a ring-shaped tuff rim and steep slopes. These maars have flat crater floors separated by well-marked knick lines from the inner slopes. They correspond to stages A, B of Büchel (1993) and stage 1 of Németh (2001).
II. Well recognizable maars but with no tuff rim or only indistinct remains. There is a smooth transition from

Table 2 Morphological parameters of known maars

Nr	Locality	Age (ka)	Source[a]	Method	*D*. Diameter (m)	*H*. Elevation (m)	Mean inner slope of crater wall (degree)	Maximum slope	Standard deviation of slope
Group I									
199	Hitsche M.	>12.4	2	P	131	7	5.1	5.3	0.1
54	Papenkaule				266	41	10.8	22.0	4.2
202	Dürres M.	>11	2	p	335	17	5.9	8.7	1.2
211	Hinkels M.	>17	2	p	336	39	10.7	20.7	4.5
200	Strohner M.	8.8	2	p	342	21	7.9	17.8	3.9
203	Holzmaar	28	1		434	27	9.7	18.9	4.1
209	Sprinker M.	>24	1	C^{14}	459	85	19.9	29.8	6.5
153	Ulmener M.	7.3–12.4	2	p	493	65	14.4	33.8	8.1
177	Gemündener M.	18	1	C^{14}	579	105	20.7	36.9	9.1
234	Booser E-M.	35	1	C^{14}	624	81	13.1	24.0	5.2
178	Weinfelder M.	10.5	2	P	665	73	15.3	28.3	6.5
201	Immerather M.	>3	1	C^{14}	692	70	13.3	24.6	4.9
196	Immerather Risch M.				735	79	11.8	23.5	5.4
179	E' Langfuhr				791	99	13.1	25.9	5.8
226	Booser W-M.	>25	1	C^{14}	848	82	10.2	27.5	5.4
181	Schalkenmehrener M.	>25	1	C^{14}	899	89	14.7	27.8	6.3
197	Pulver M.	>7	1	C^{14}	921	58	14.8	24.3	5.7
188	Mürmes	>12.5	1	p	1,055	41	7.5	17.8	3.2
236	Moosbrucher M.	14.0	1	p	1,083	97	10.2	19.7	4.4
74	Dreiser Weiher M.	>27	1	C^{14}	1,278	108	11.4	26.8	5.4
210	Meerfelder M.	41.3	1	C^{14}	1,578	183	19.3	32.7	7.7
	$\Sigma = 21$								
Group II									
243	M. am Schäferhof				216	27	9.4	12.4	1.9
70	NW' auf Erbenschell				260	55	13.6	22.6	4.7
205	Trautzberger M.	>20	2	p	285	32	9.1	17.0	3.6
75	SW' Gonnenstall				347	58	11.8	22.1	3.8
96	M. am Römerhof				444	34	7.6	15.7	3.0
187	M. am Hohen List		1	C^{14}	455	35	8.8	16.9	2.8
249	Neunkirchner M.				460	76	11.7	21.7	4.5
238	Säupersch M.				461	52	8.5	13.4	2.2
189	Wollmerather M.				480	55	8.2	14.6	2.7
27	Duppacher Weiher	>26	1	C^{14}	551	31	9.6	15.0	2.7

Table 2 continued

Nr	Locality	Age (ka)	Source[a]	Method	*D*. Diameter (m)	*H*. Elevation (m)	Mean inner slope of crater wall (degree)	Maximum slope	Standard deviation of slope
59	Lierwiesen-M.				552	38	6.3	11.0	1.7
128	W' Ringseitert				629	33	5.2	8.7	0.9
165	Oberstadtfelder M.				638	117	14.4	27.8	7.3
192	Ellscheider M.	>27	1	C^{14}	679	29	6.7	13.1	2.4
29	Duppacher M.				690	89	9.4	20.9	4.5
92	Hohenfelser M.	660 ± 80	4	40Ar/39Ar	716	76	9.3	18.3	3.0
8	Merscheider M.	>37	1	C^{14}	771	41	7.3	19.2	2.6
194	Oberwinkler M.	>52.6	1	C^{14}	800	44	7.3	19.6	3.0
68	Brücker S.	45	1	C^{14}	820	61	6.9	16.7	2.4
106	In der Boos				844	37	5.1	10.7	1.0
156	Eigelbacher M.	140	1	C^{14}	862	98	10.1	21.7	3.7
184	M. W' Hoher List	132	1	C^{14}	926	70	7.2	15.3	2.5
7	Dehner	130	1	C^{14}	931	56	6.5	12.2	2.0
67	Walsdorfer M.	>135	1	C^{14}	979	63	6.9	16.8	2.4
	$\Sigma = 25$								
Group III									
174	Eckfelder M.	44,300	3	40Ar/39Ar	198	53	10.0	21.3	4.0
239	Eichholzmaar				258	20	7.2	12.9	2.6
175	SW' Buerberg	345 ± 1.8	4	40Ka/40Ar	345	111	20.0	31.5	7.7
183	Steineberger M.				421	33	6.2	10.1	1.4
250	M. N' Steinborn				442	33	7.4	12.7	2.1
256	Döttinger S.				452	34	6.6	11.3	2.0
221	Hardt M.				485	141	20.5	36.4	9.2
44	NNE' Wiesenhof				495	27	6.0	11.6	1.8
77	Essinger M.				501	51	7.7	12.3	1.9
164	NNW' Wallenborn				542	62	9.8	18.1	3.6
244	Rockeskyll T.	360 ± 40	4	40Ka/40Ar	551	63	10.4	23.4	4.5
39	ESE' Wolfsbeuel?				570	46	5.8	13.0	1.3
251	Neunkirchener T.				602	63	7.4	14.3	2.2
244	M. N' Pelm				611	40	9.5	19.1	3.7
55	S' Wöllersberg				634	59	9.6	29.9	5.8
166	Niederstadtfelder T.	>37	1	C^{14}	650	35	6.2	12.7	1.8
136	Hippersbach				654	94	9.7	25.0	4.3
245	Seiderather M.				779	95	10.2	25.2	4.1

Table 2 continued

Nr	Locality	Age (ka)	Source[a]	Method	*D*. Diameter (m)	*H*. Elevation (m)	Mean inner slope of crater wall (degree)	Maximum slope	Standard deviation of slope
182	Mehrener M.	>32	1	C^{14}	786	34	6.1	12.5	1.7
148	Hengstweiler M.	>16	1	C^{14}	786	88	11.7	24.4	4.7
246	Gyppenberger T.				827	100	13.8	27.4	5.9
134	Steinborner M.	>60	1	?	869	47	5.8	9.0	1.2
247	Pelmer T.				933	97	11.8	31.0	5.7
115	Kirchweiler M.				963	29	5.3	9.7	1.1
10	Laach-M.				1,016	52	6.9	17.0	2.3
132	Geeser M.				1,069	125	13.1	31.4	5.0
255	Döttinger M.	390	1	?	1,291	59	6.0	16.0	1.8
15	Auel M.	>30	1	C^{14}	1,293	45	5.4	10.4	1.2
	$\Sigma = 27$								
Group IV									
5	W' Basberg M.	524 ± 197	4	40Ar/39Ar	242	16	6.8	10.6	1.5
98	In der Eyd-W?				368	37	6.6	14.8	2.1
252	Dauner M.?				390	22	4.8	7.4	0.9
38	SW' Wolfsbeuel?				402	14	4.0	4.0	0.0
3	Kerpener M.				460	20	6.3	11.1	1.9
241	M. SW' Roth				467	13	4.5	4.8	0.2
35	E' Loscheid				475	17	4.6	5.7	0.5
2	Schönfelder M.	>39	1	C^{14}	506	31	7.1	10.2	1.5
13	E' Steffeln				652	63	7.7	16.7	3.1
240	Steffelner M.				714	42	6.4	16.9	2.5
34	Rother M.	>34	1	C^{14}	823	49	5.9	9.9	1.3
46	Gerolsteiner M.				1,028	46	6.8	14.9	2.1
257	Jungfer Weiher	132	1	C^{14}	1,562	26	4.5	5.2	0.4
	$\Sigma = 15$								
Group V									
217	Kennfuser M.				230	31	9.0	15.8	4.1
17	Killenberg?				283	43	9.3	16.0	2.9
237	Elfen M. (D)				301	90	17.6	30.2	7.2
91	Burlich				308	65	17.6	31.1	6.5
193	Weidgert				310	73	14.0	26.3	6.0
26	SE' Bolsdorf				334	24	5.3	7.5	0.9
93	Nohn (SSW' Betteldorf)				343	44	8.7	15.8	2.3

Table 2 continued

Nr	Locality	Age (ka)	Source[a]	Method	*D*. Diameter (m)	*H*. Elevation (m)	Mean inner slope of crater wall (degree)	Maximum slope	Standard deviation of slope
69	SSE' Kyller Höhe	457 ± 129	4	40Ar/39Ar	368	37	7.2	13.4	2.4
89	SW' Rockeskyll	360 ± 40	4	40Ka/40Ar	565	40	6.8	12.6	2.0
78	Auf Dickel				657	56	9.2	21.5	4.1
	Σ = 10								

Nr	Locality	Ratio of crater wall area over crater floor area	*S* Assumed sediment thickness (m) (1: 11 of diameter)	Relation $D/(H + S)$	Isometric local depression[b]	Concavity[c]	Isometric areas of river junction density >3/600 m^2	Area containing more than 7 linear river segments/500 m^2	Bifurcating river patterns
Group I									
199	Hitsche M.	2.3	11.9	6.9	–	+	–	–	–
54	Papenkaule	1.0	24.2	4.1	–	+	–	–	–
202	Dürres M.	1.5	30.4	7.1	++	+	–	–	–
211	Hinkels M.	1.3	30.5	4.8	–	+	–	–	–
200	Strohner M.	1.7	31.1	6.5	++	+	–	–	+
203	Holzmaar	1.6	39.4	6.5	+	++	+	+	+
209	Sprinker M.	1.2	41.8	3.6	++	++	+	–	+
153	Ulmener M.	1.3	44.8	4.5	++	+	–	–	–
177	Gemündener M.	1.2	52.6	3.7	++	+	+	+	+
234	Booser E-M.	1.2	56.8	4.5	++	+	–	–	+
178	Weinfelder M.	1.7	60.5	5.0	++	++	+	+	+
201	Immerather M.	1.2	62.9	5.2	++	++	+	+	+
196	Immerather Risch M.	1.5	66.8	5.0	++	++	+	+	+
179	E' Langfuhr	1.2	71.9	4.6	++	++	+	–	–
226	Booser W-M.	1.3	77.1	5.3	++	++	+	+	+
181	Schalkenmehrener M.	1.7	81.7	5.3	++	+	+	+	+
197	Pulver M.	1.9	83.8	6.5	++	++	+	+	+
188	Mürmes	2.3	95.9	7.7	++	++	+	+	+
236	Moosbrucher M.	1.5	98.4	5.5	++	++	+	+	+
74	Dreiser Weiher M.	1.7	116.2	5.7	++	++	+	+	+
210	Meerfelder M.	1.4	143.5	4.8	++	++	+	+	+
	Σ = 21								

Table 2 continued

Nr	Locality	Ratio of crater wall area over crater floor area	*S* Assumed sediment thickness (m) (1: 11 of diameter)	Relation $D/(H + S)$	Isometric local depression[b]	Concavity[c]	Isometric areas of river junction density >3/600 m^2	Area containing more than 7 linear river segments/500 m^2	Bifurcating river patterns
Group II									
243	M. am Schäferhof	1.1	19.6	4.7	–	+	–	–	–
70	NW' auf Erbenschell	1.0	23.7	3.3	+	+	–	–	–
205	Trautzberger M.	1.2	25.9	4.9	++	+	–	–	+
75	SW' Gonnenstall	1.0	31.5	3.9	++	+	–	–	–
96	M. am Römerhof	1.4	40.4	6.0	++	++	+	+	+
187	M. am Hohen List	1.1	41.4	5.9	++	+	+	+	+
249	Neunkirchner M.	1.0	41.9	3.9	+	+	–	–	+
238	Säupersch M.	1.1	41.9	4.9	++	+	+	–	+
189	Wollmerather M.	1.1	43.7	4.8	++	++	+	+	+
27	Duppacher Weiher	1.8	50.1	6.8	++	++	+	+	+
59	Lierwiesen-M.	1.7	50.2	6.2	++	++	+	+	+
128	W' Ringseitert	2.4	57.2	7.0	++	++	+	+	+
165	Oberstadtfelder M.	1.0	58.0	3.6	++	++	+	+	+
192	Ellscheider M.	1.9	61.7	7.5	++	++	+	+	+
29	Duppacher M.	1.2	62.7	4.5	++	++	+	+	+
92	Hohenfelser M.	1.1	65.1	5.1	–#	++	+	+	+
8	Merscheider M.	1.6	70.1	7.0	++	++	+	+	+
194	Oberwinkler M.	1.8	72.7	6.9	++	++	+	+	+
68	Brücker S.	1.4	74.6	6.1	++	++	+	+	+
106	In der Boos	1.9	76.7	7.4	++	++	+	+	+
156	Eigelbacher M.	1.0	78.3	4.9	++	++	+	+	+
184	M. W' Hoher List	1.2	84.2	6.0	++	++	+	+	+
7	Dehner	1.8	84.6	6.6	++	++	+	+	+
67	Walsdorfer M.	1.7	89.0	6.4	++	++	+	+	+
	$\Sigma = 25$								
Group III									
174	Eckfelder M.	38.5	18.0	2.8	+	+	+	–	+
239	Eichholzmaar	1.5	23.4	5.9	–	+	+	–	–
175	SW' Buerberg	1.1	31.4	2.4	–	+	–	–	–
183	Steineberger M.	1.1	38.3	5.9	++	++	+	+	+
250	M. N' Steinborn	1.2	40.2	6.0	+	++	–	+	+

Table 2 continued

Nr	Locality	Ratio of crater wall area over crater floor area	*S* Assumed sediment thickness (m) (1: 11 of diameter)	Relation $D/(H + S)$	Isometric local depression[b]	Concavity[c]	Isometric areas of river junction density >3/600 m^2	Area containing more than 7 linear river segments/500 m^2	Bifurcating river patterns
256	Döttinger S.	1.7	41.1	6.1	–	–	–	+	–
221	Hardt M.	1.0	44.1	2.6	–	+	–	+	+
44	NNE' Wiesenhof	2.5	45.0	6.9	+	+	+	–	+
77	Essinger M.	1.2	45.5	5.2	–	+	+	–	–
164	NNW' Wallenborn	1.0	49.3	4.9	–	+	–	+	+
244	Rockeskyll T.	1.1	50.1	4.9	–	+	+	+	–
39	ESE' Wolfsbeuel?	1.1	51.9	5.8	+	+	+	+	+
251	Neunkirchener T.	1.3	54.7	5.1	–	+	–	+	+
244	M. N' Pelm	2.2	55.6	6.4	–	+	+	+	+
55	S' Wöllersberg	1.4	57.6	5.4	–	+	–	–	+
166	Niederstadtfelder T.	1.6	59.1	6.9	+	++	+	–	+
136	Hippersbach	1.1	59.4	4.3	–	+	+	+	+
245	Seiderather M.	1.1	70.8	4.7	+	+	+	+	+
182	Mehrener M.	2.1	71.5	7.4	++	++	+	+	+
148	Hengstweiler M.	1.1	71.5	4.9	++	++	+	+	+
246	Gyppenberger T.	1.1	75.2	4.7	–	+	–	+	+
134	Steinborner M.	1.7	79.0	6.9	+	++	+	+	+
247	Pelmer T.	1.4	84.8	5.1	+	+	+	+	+
115	Kirchweiler M.	3.5	87.6	8.3	–	++	+	+	+
10	Laach-M.	1.6	92.3	7.0	+	+	+	+	+
132	Geeser M.	1.0	97.2	4.8	+	+	+	+	+
255	Döttinger M.	1.9	117.3	7.3	–	++	+	+	+
15	Auel M.	2.6	117.6	7.9	+	+	+	+	+
	$\Sigma = 27$								
Group IV									
5	W' Basberg M.	1.9	22.0	6.3	–	+	–	–	–
98	In der Eyd-W?	1.1	33.4	5.2	–	+	–	–	+
252	Dauner M.?	1.8	35.5	6.8	+	+	–	+	+
38	SW' Wolfsbeuel?	80.0	36.6	7.9	++	+	–	–	–
3	Kerpener M.	2.6	41.9	7.4	–	+	–	+	+
241	M. SW' Roth	26.8	42.5	8.4	++	++	+	+	+
35	E' Loscheid	4.9	43.2	7.9	++	+	–	–	+
2	Schönfelder M.	2.1	46.0	6.6	++	++	+	+	+

Table 2 continued

Nr	Locality	Ratio of crater wall area over crater floor area	*S* Assumed sediment thickness (m) (1: 11 of diameter)	Relation $D/(H + S)$	Isometric local depression[b]	Concavity[c]	Isometric areas of river junction density >3/600 m^2	Area containing more than 7 linear river segments/500 m^2	Bifurcating river patterns
13	E' Steffeln	1.6	59.3	5.3	+	++	+	+	+
240	Steffelner M.	2.0	64.9	6.6	++	++	+	+	+
34	Rother M.	2.2	74.8	6.6	++	++	+	+	+
46	Gerolsteiner M.	1.6	93.5	7.4	++	++	+	+	+
257	Jungfer Weiher	52.2	142.0	9.3	++	++	+	+	+
	$\Sigma = 15$								
Group V									
217	Kennfuser M.	1.3			+	–	–	–	–
17	Killenberg?	1.1			–	–	–	–	–
237	Elfen M. (D)	1.1			–	+	–	–	–
91	Burlich	1.0			–	+	+	+	–
193	Weidgert	1.0			+	+	–	–	–
26	SE' Bolsdorf	1.9			–	+	–	–	–
93	Nohn (SSW' Betteldorf)	1.0			+	+	–	+	–
69	SSE' Kyller Höhe	1.2			–	+	+	+	–
89	SW' Rockeskyll	1.3			–	–	–	–	–
78	Auf Dickel	1.6			–	+	–	–	–
	$\Sigma = 10$								

[a] Schaber and Sirocko (2005), Meyer (1994), Pirrung et al. (2003), Nowell et al. (2006)

[b] ++ Contours of isometric local depression coincide with known maars, + Contours of isometric local depression partially coincide with known maars, # Local depression overlapping with other maars

[c] ++ Ring-shaped pattern of concavity values, + Concavity values coinciding with known maars

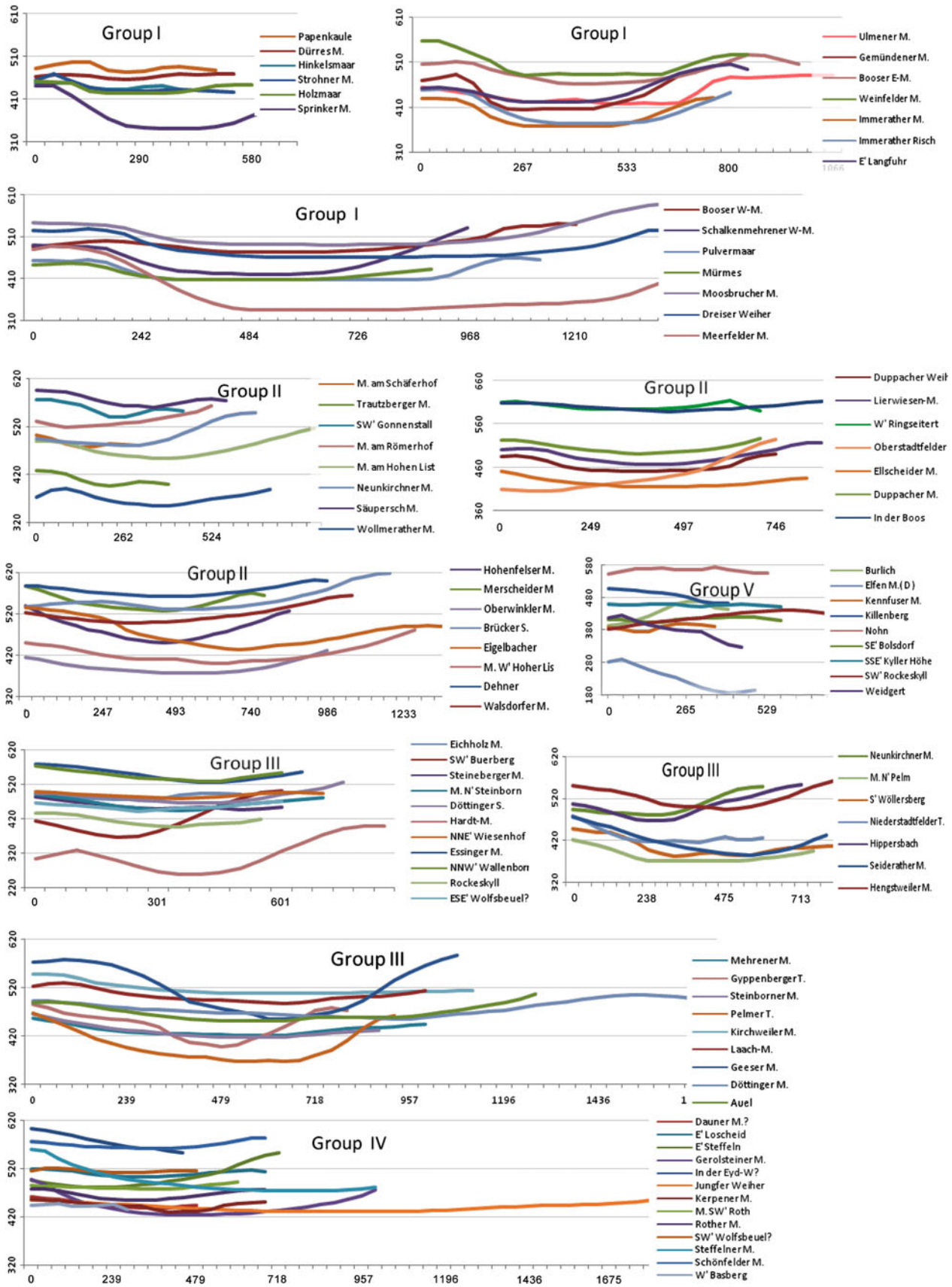

Fig. 3 The five groups of profile shapes for maars and similar volcanoes distinguished in this paper

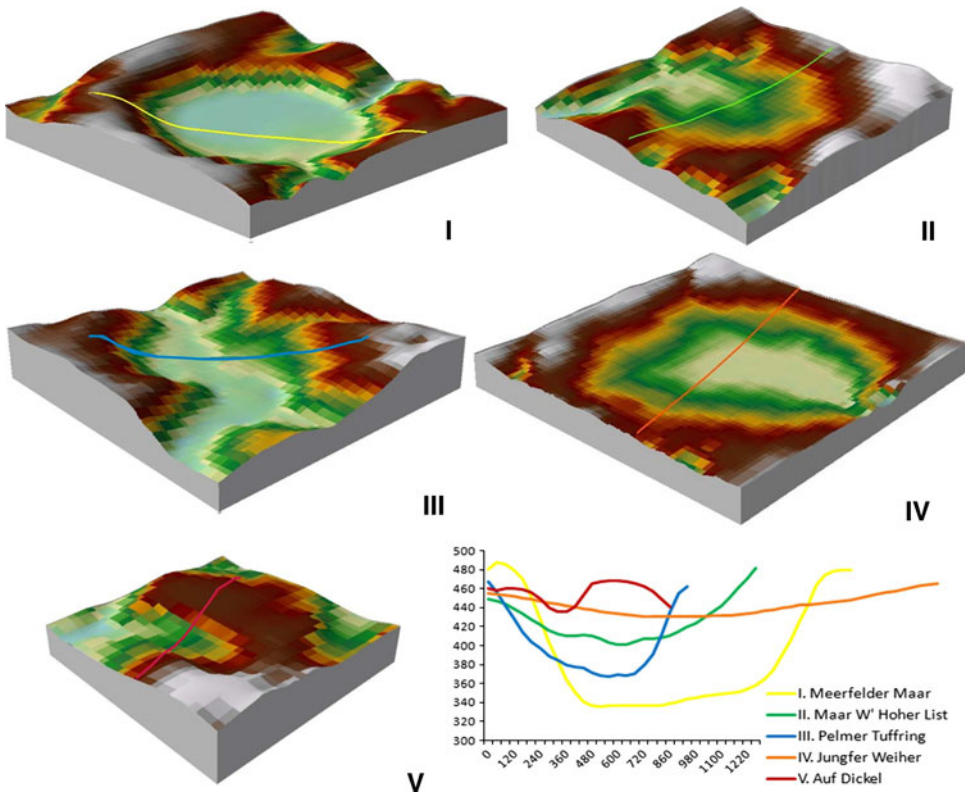

Fig. 4 Representatives of typical shapes and typical profiles for each morphometric group. Further explanations in the text

crater floors to inner slopes. These correspond to stage D of Büchel (1993).

III. Maars whose shape has been complicated by fluvial erosion. These types can often be recognized from particular geometries of the drainage network.

IV. Very shallow depressions which can hardly be recognized in the landscape. Most of these were only identified as maars through geophysical investigations. This group is equivalent to class C of Büchel (1993).

V. Deeply eroded maars transformed into positive landforms by relief inversion. These correspond to stage E of Büchel (1993) and stage 3 of Németh (2001).

Some maars overlap, creating complex forms. Such maars were classified on the basis of profiles across those parts unaffected by the adjacent maar (Fig. 5a).

There is no linear correlation between our morphological classification and the erosion stages defined by Büchel and Németh, respectively. Only Group I always corresponds to recent maars (Fig. 5b). Groups II to V comprise both recent and older maars.

Definition of search criteria

In the West Eifel Volcanic Field, Group V only comprises 6 small tuff rings, 2 scoria rings, and 2 maars. Most of them are particularly small and indistinct. We therefore did not use the structures of Group V in our definition of search criteria. Group I to IV structures were used to define maar characteristics.

Groups I, II, and IV comprise clear ring-shaped structures. In an ideal circle, the radius calculated from the perimeter of the contour (R_p) is equal to the radius calculated from the area (R_a) bounded by this contour and the ratio of these values—*the circular ratio*—is one ($R_a/R_p = M = 1$). The circular ratio will be reduced by irregularities of the circle. We expect the landforms of Groups I, II, and IV to be separated from other local depressions by calculation of their circular ratios (Zăvoianu 1985). The difference between the groups is that a tuff rim is well preserved in Group I and partially preserved in Group II. The original shapes of Group III maars have been altered more substantially compared to Groups I, II, or IV, but they nevertheless retain a negative shape and have characteristic channel systems, which can be used as search criteria.

Digital Terrain data and GIS allow to rapidly extract morphological properties of maars and statistically analyze them (Table 2).

Table 2 shows that the diameters of the maars of the West Eifel Volcanic Field range from 83 to 1,580 m. Diameters were calculated as $D = 2 \times \sqrt{S/\pi}$, where D is the diameter and S the area of the horizontal projection of the surface bounded by the external contour of a maar. Elevation differences from crater rim to crater floor range

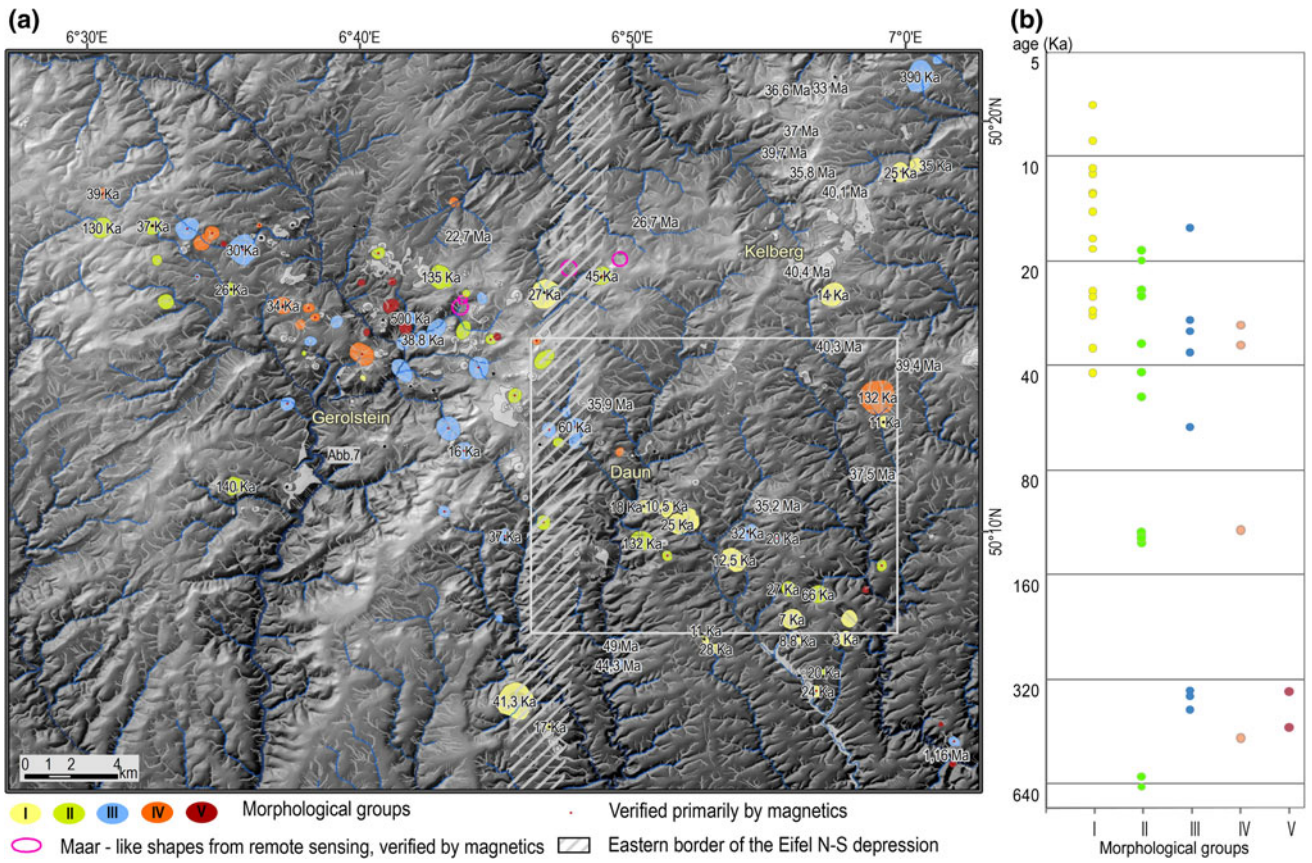

Fig. 5 **a** Spatial distribution of the five groups of maar-forming volcanoes. **b** Age distribution in the morphological groups

from 6 to 183 m. Maximum slope of the crater rim is 36.9° in the Gemündener Maar (Table 2).

Analysis of the maar shapes reveals several main geometric features:

- Low, constant slope (0°–4°) of the crater floor which is smoothed by sediment or water infill.
- Slopes values ranging from 5° to 36° on crater rims.
- Maxima in surface curvature corresponding to crater rims. These can be obtained from the DTM as maxima of either of longitudinal curvature or of maximum profile of surface raster (Wood 1996).
- Minima of profile curvature indicating knick lines between the rim slopes and crater floors or surroundings, respectively. These are characteristic of young maars.
- Circular contour lines revealing closed, bowl-shaped depressions
- Constant density of the (calculated) drainage system.

On the basis of this analysis, we have to search for circular negative landforms with slope angles up to 30°, knick lines between slopes and floors or surrounding areas and arcuate scarps probably related to compaction of maar sediments. An additional criterion is dense drainage systems with a characteristic pattern.

The extraction of maar landforms then involves the following steps:

- a residual relief is calculated as the difference between original and smoothed elevation models;
- circular and elliptical contours are extracted from the residual relief according to defined circularity ratios;
- slope angles of rims and floors are taken from the slope raster;
- all knick lines are extracted from the profile curvature raster;
- crater rims are extracted from the maximum curvature raster;
- a query is performed for areas where the density of the drainage network exceeds a defined value.

Data processing

Modern software packages provide several operations for nearly automated extraction of landscape elements from DTMs. However, more complex operations require several steps. This is true of the residual relief and further analyses based thereon. These calculations involve several parameters explained below. The workflow is shown in Fig. 7.

Data and programs used

The Digital Terrain Model 50 (DTM 50) represents the topography of the earth's surface through a regular point raster where each point is defined by horizontal coordinates and an elevation value. The DTM 50 was created in 1990 from the elevation contour lines of the 1:50,000 German topographic map (Transversal Mercator projection, datum Bessel 1841). It has a 25 m × 25 m raster and elevations are typically accurate to ±4–6 m. Only exceptionally the accuracy may drop to ±25 m (TLVermGEO). For the present study, data were acquired from the Bundesamt für Kartographie und Geodäsie (Federal Agency for Cartography and Geodesy). The data were delivered as ASCII files and transformed into raster data using kriging in ArcMap. It is a thematic raster of 45 km × 36 km size comprised between longitudes E6°26′ and E7°4′ and latitudes N50°2′ and N50°22′. Pixel size is 40 m. Each Pixel is assigned a value of absolute elevation.

The DTM data were processed using the software packages ENVI 4.3 (RSI) and ArcGIS 9.1 (ESRI). From the ArcGIS package, we used the modules 3D Analyst, Spatial Analyst, ET GeoWizards, EasyCalculate, and ArcMap.

Drainage network

Maars affected by fluvial erosion rapidly lose their ring shape. However, characteristic densifications of the channel network and clustered junctions of channels of similar size still indicate the presence of maars. The drainage network was extracted from *digital* elevation models using the ArcHydro module, with the tolerance for stream capture set to 10 pixels. The rivers were assigned orders according to Strahler (1952, 1957). The obtained drainage network coincides well with the natural network (Fig. 8), except for some tributaries and obvious artifacts on the flat maar crater floors. There, the drainage network exhibits closely spaced parallel channels (e.g., Pulver Maar and Jungferweiher Maar). However, since these very artifacts highlight flat crater floors, we decided not to eliminate them before further calculations were made. In the simulated drainage network, we defined as junctions all nodes except those at the origins or ends of channels (Fig. 8), which were not used in the following calculations. For the simulated river network, we calculated the density of channels and of channel junctions per area. Regions with more than 7 channels per 500 m^2 were selected and converted to outlines (Fig. 9d), and so were regions with more than 4 junctions per 600 m^2. Many known maars coincide with roughly circular regions of increased junction density. We therefore converted the closed outlines to polygons and selected those with a circular ratio of more than 0.81. The areas thus selected match well with several maars, particularly those of the 3rd group (maars with forms modified by fluvial erosion) (Fig. 9f).

Residual relief

Active uplift of the Eifel region has led to accelerated erosion of volcanic edifices and modification of their original shapes. Maars located in valleys were affected differentially by river incision and their shapes have become similar to the surrounding erosional landforms. This hampers their identification on topographic maps. Extracting local depressions from the DTM is a means of identifying the potential locations of covered and eroded maars. In order to select local depressions, a generalized surface model must be created and the DTM subtracted from it. In our case, the surface model is a surface connecting ridges of the DTM. Fitting of the surface to the ridges was done with variable tolerance, depending on the order of ridges taken into account.

Natural maars have several small ridges within their craters. In order to obtain the complete shape of a maar depression, these ridges should be ignored while the crater rim should be represented with the highest precision possible (Fig. 6). Several variants with different tolerance parameters were tested to arrive at an optimal solution. The criterium for the best set of tolerance parameters was the match between the topographic anomalies isolated after processing a known maars. Each variant tested led to enhanced identification of some maar groups, but none led to optimum results for all groups. The steps for one variant were the following:

1. Using ENVI, ridges and channels were extracted. According to Wood (1996), ridges are composed of points exhibiting local convexity perpendicular to a line with no convexity or concavity:
$$\frac{\delta^2 z}{\delta x^2} > 0, \quad \frac{\delta^2 z}{\delta y^2} = 0$$
Likewise, channels comprise points exhibiting local concavity perpendicular to a line with no concavity or convexity:
$$\frac{\delta^2 z}{\delta x^2} < 0, \quad \frac{\delta^2 z}{\delta y^2} = 0$$
2. Using ArcMap, a base surface was created from the extracted channels (Grohmann et al. 2007).
3. For the ridges, elevations relative to the base surface were calculated.
4. Ridges higher than a defined threshold elevation were selected.
5. Absolute elevation values were assigned to the points on the selected ridges.

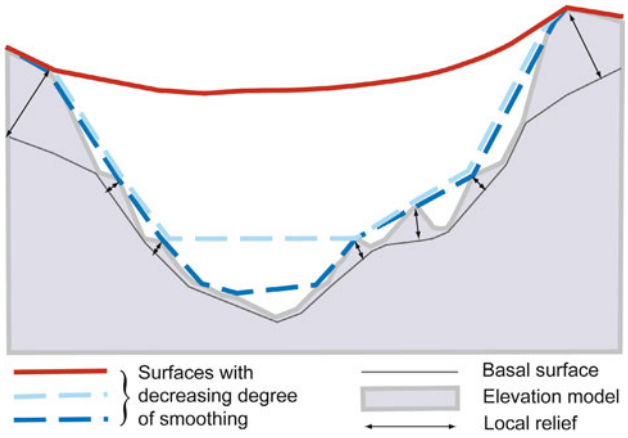

Fig. 6 Generalized land surfaces with different degrees of smoothing (*red*, *blue*, *light blue*). Profile of the base surface (*thin gray line*) and distance of ridges from the base surface (*black arrows*)

6. A surface was created from the points using the natural neighbor interpolation method implemented in ArcMap Tools.
7. Finally, the new surface was subtracted from the elevation model to obtain a new residual surface in which the local depressions stand out (Fig. 9a).

Alternatively, the elevation raster was smoothed using a 5 × 5 pixel low pass filter. Then, elevation values of pixels with a maximum curvature higher than 0.5 were replaced by the original values. The new interpolated raster was subtracted from the elevation surface. This workflow enhanced the shapes of maars but also separated many small shapes, thereby strongly increasing noise.

Slope

Slope is calculated as the first derivative of the elevation model (Wood 1996). It corresponds to the maximum elevation change over a given distance and is indicated in degrees. A 3 × 3 pixel window was used to calculate a slope value for each pixel according to the following equation:

$$\text{Slope} = \arctan\sqrt{d^2 + e^2}$$

(Wood 1996; Roberts 2001) where

$$d = (z3 + z6 + z9 - z1 - z4 - z7)/6g$$
$$e = (z1 + z2 + z3 - z7 - z8 - z9)/6g$$

and z1 to z9 are pixels in the 3 × 3 pixel matrix as follows:

z1	z2	z3
z4	z5	z6
z7	z8	z9

Values of the slope raster smaller than 30° were selected and combined with the curvature and residual elevation rasters.

Profile convexity

Profile convexity is calculated for a vertical profile of the surface in the direction of the inclination and indicates the change in slope (intersecting with the plane of the Z axis and aspect direction). It corresponds to the second derivative of the elevation raster or the first derivative of the slope (Evans 1979; Wood 1996; Roberts 2001). Profile convexity is calaculated according to the following equation:

$$\text{profc} = \frac{-200(ad^2 + be^2 + cde)}{(e^2 + d^2)(1 + d^2 + e^2)^{1.5}}$$

(Wood 1996) where

$$a = (z1 + z3 + z4 + z6 + z7 + z9)/6g2 - (z2 + z5 + z8)/3g2$$
$$b = (z1 + z2 + z3 + z7 + z8 + z9)/6g2 - (z4 + z5 + z6)/3g2$$
$$c = (z3 + z7 - z1 - z9)/4g2$$

The profile convexity raster was created using ENVI's topography module. Values smaller than −0.05 correspond to concave positions and knick lines within depressions (Fig. 9b).

Maximum of profile curvature

The maximum curvature method identifies maxima of the profile convexity raster. In each case, the highest gray value in a 3 × 3 surrounding of the Profile Convexity matrix forms a local maximum. The maximum curvature raster was also created using ENVI's topography module.

The maximum of profile curvature is calculated as:

$$\text{profc max} = -a - b + \sqrt{(a - b)2 + c2}$$

(Wood 1996).

Contour lines

Contour lines were created from the new residual relief at 2 m intervals (Fig. 9c). From our analysis of maar characteristics, the maximum perimeter of a single maar would be $D \times \pi = 1{,}580 \times \sim 3.14 = \sim 5{,}000$ m. Overlapping maars could have three times that perimeter value (~15,000 m). All closed contours with a higher perimeter can already be eliminated in this processing stage. The shortest contour was chosen to be no smaller than 2 pixels × π = 2 × 40 m × ~3.14 = ~251.2 m. All contours with perimeters between 252 and 15,000 m were transformed into areas using ET GeoWizards of ArcGIS.

The areas were then selected according to size and circular ratio M:

$$M = 4\pi \times \text{area}/\text{perimeter}^2$$

(Zăvoianu 1985).

Areas narrower than 400 m were selected if their circular ratio (M) exceeded 0.85. Those wider than 400 m were selected if M exceeded 0.6. Thus, all roughly circular local depressions were separated (Fig. 9e). Unfortunately, this method eliminates some negative shapes that might be of maar origin. Visual analysis of these shapes suggests they represent several overlapping isometric volcanic forms (Figs. 10b, 11g). Also, maar shapes elongated in one direction by fluvial erosion were lost (Fig. 10, Gyppenberger Maar).

Processing results

We processed digital elevation data to obtain the following new datasets:

1. A *residual relief* surface which enhances all local negative landforms (Fig. 9a).
2. A concavity raster, identifying points where *profile curvature* is less than −0.05 (Fig. 9b).
3. A slope *raster for slopes* between 5° and 16°.
4. A *maximum curvature raster*.
5. A shape file of local depressions having *circular ratios* more than 0.85 (for small depressions) and more than 0.6 (for large depressions) (Fig. 9e).
6. A shape file of areas where the drainage network has more than 4 junctions per 600 m, and circular ratio of more than 0.81 (Fig. 9f).
7. A shape file of contoured areas where the drainage network has more than 7 channels per 500 m. (Fig. 9d).

Discussion

Complex landform analysis

The use of DTM data allows to automatically extract several parameters of the maars. The spatial limits of maars used in the evaluation of their properties were taken from the Volcanological map West- and Hocheifel (Büchel 1994). Within the maar contours, the DTM raster surface was transformed to points, and values for slope and elevation were calculated (Fig. 2). Areas with slope angles below 4° were defined as floors, areas with slope angles above 4° as slopes. The maar depth was calculated as the difference between maximum and minimum elevation values. The thickness of marginal crater sediments was assumed to be 1/11 of the crater diameter following Schaber and Sirocko (2005). This sediment thickness was taken into account in the calculation of the diameter to hight ratio. Some statistical properties of the maars can be summarized as follows (Table 3):

While most of the Group I maars are dated, age data exist for only 10 out of 23 maars in Group II. For some of the undated volcanoes (Trauzberger, Duppacher, Ellscheider, Merscheider and Oberwinkler maars, Brücker Schlackenring), minimum ages can be obtained from estimates of the time when the maar lakes became silted up. These estimates range from 20 to 66 ka (Schaber and Sirocko 2005). The relatively strong erosion combined with young ages for some maars of this group suggests that either the minimum ages severely underestimate the true ages or the local erosion was particularly active.

Strong fluvial erosion characterizes many maars in Group III. Most of the strongly incised maars are located in the vicinity of the Kyll and Kleine Kyll rivers and their tributaries. All Group III maars are traversed by rivers (Fig. 5). The well-developed river system dissecting relatively young maars and slope angles as high as 36° suggests recent uplift that induced strong fluvial incision.

The statistical characteristics of the maars show that the most sensitive parameter for group separation is the standard deviation of slope. Maar diameters show no simple correlation with age or spatial distribution. The relation of diameter to crater depth is relatively stable at ca. 5:1 for maars with a tuff ring and ca. 7:1 for maars without tuff ring if crater sediments are taken into account. These values can be used to reconstruct the shapes of eroded maars and estimate the amounts of erosion.

Table 3 Morphological parameters of the five morphometric groups in the West Eifel Volcanic Field as defined in this paper

Groups	Age from–to (ka)	Slope of crater wall (°)		Standard deviation of slope (°)			Elevation		Diameter		
		Max	Mean	Min	Max	Mean	Max	Mean	Min	Max	Mean
I	3–41	37	12	0.8	9	5	183	70	131	1,578	700
II	20–140	28	8	0.9	7	3	117	56	260	980	633
III	16–500	36	9	0.7	9	3.3	141	56	83	1,293	690
IV	34–39	17	6	0	3	1.4	63	30	242	1,562	622
V		23	10	0	7	1.9	90	50	230	656	370

Maars of Group I which possess a tuff ring differ in age by as much as 50 ka, yet their shapes show no significant differences. Most maars of the first group lie east of the ENSZ. At the same time, we can find maars less than 40 ka old in the other, more severely eroded groups. Some young maars, such as the 30 ka old Auel Maar or the 34 ka old Rother Maar, are almost flat.

On the other hand, some Tertiary maars as old as 44 Ma are remarkably well preserved. If we assume an original diatreme depth of 2 km, very low (<0.045–0.06 mm per year) average rates of erosion result compared to other areas with maar-diatremes of Tertiary or Quaternary age.

All known maars corresponding to depressions were clearly visualized in the first two rasters although on the ground some of them had only been detected using geophysical measurements. An even better visualization was obtained with a RGB combination of the residual relief, concavity and slope rasters or residual relief with shaded relief and maximum curvature (Fig. 9g). The concavity raster was further reduced for additional analysis, taking into account only pixels where the slope angle is less than 30°.

The maars of Groups I, II, and IV often exhibit characteristic ring patterns in the profile curvature raster (marked as "++" in Table 2). Maars of Group III are indistinct in the concavity raster. They show concavity only where traversed by channels (i.e., Steinborner Maar).

The residual relief created using the method described above partially removes the effects of fluvial erosion. Therefore, 52 % of the Group III maars are captured by the circular contour criterion. Within Groups I, II, and IV, only 7 maars of small size (diameter < 370 m = 9 pixels) were omitted. Thus, 88.5 % of the maars in Groups I, II, and IV were automatically selected by our new method. Somewhat surprisingly, the shallow Group IV maars were recognized to the same degree as the better preserved maars of Groups I and II.

The automatic recognition of Group III maars was markedly improved by searching for circular contours created from the river junction density raster. This resulted in a recovery of 20 maars (74 %) out of Group 3. The method also worked well on Group II maars (80 % recovery) and only slightly less efficiently on Groups I and IV (recovery of 61 and 60 %, respectively). The contours of the drainage network density can be used as an additional criterion. Density highs often coincide with maars, but do not have clear circular shapes.

A query for concavity values coinciding with circular contours of the residual relief and with circular drainage network density anomalies selects all known negative maar shapes and several similar shapes, many of which could represent unmapped maars. This is borne out by measurements of magnetic anomalies indicating a maar origin for some structures identified from DTM data (Seib et al. 2008). Most maars exhibit arc patterns in the concavity raster and drainage patterns bifurcating in a specific way (Figs. 8, 9, 10). The slope and maximum curvature rasters highlight the annular rims of maar structures and can be used to search for unknown maars.

Each processing method used and their combination enhance the visualization of the positions of known maars and similar structures. Figure 10 shows how anomalies obtained with the different methods correlate with mapped maars in a selected area. Figure 11 shows newly recognized maar-forming structures exhibiting several characteristic features. There are clear analogies with mapped maars (Fig. 7). Figure 12 shows all anomalies obtained through the methods described above. The new features can be used to guide future field work or magnetic surveys.

Ages of maars and erosion rates

The majority of the erosion of tephra rings takes place during eruption and a period of days to weeks afterward (Németh 2003; Lorenz 2003; Pirrung et al. 2008). Intense landsliding and collapse of the tephra ring may go on for several years (Pirrung et al. 2008). This is the most intense period of maar erosion. After stabilization of the tephra ring, erosion of maars is relatively slow depending on climatic conditions, uplifting or type of rocks composing the ring and crater.

Németh (2001) and Németh and White (2003a, b) estimated the erosion rates of Miocene volcanoes in New Zealand to range from 0.037 to 0.5 mm per year. The Mio-/Pliocene Bakony-Balaton highland volcanic field has been eroding by 0.1–1 mm per year (Németh et al. 2003; Németh and Martin 1999). Degeai (2004) reconstructed the Quaternary volcanoes of the French Massif Central and derived erosion rates between 0.06 and 1.96 mm per year. Rates between 0.01 and 0.03 mm per year were calculated for South African kimberlites (Hanson 2007). Based on the erosion rates of similar regions, we assume that the erosion rates in the West Eifel Volcanic Field range from 0.03 to c. 2 mm per year.

Degeai (2004) related ages and erosion rates for maars of the French Massif Central (his Table 3), finding a general trend of higher erosion rates for younger maars. We have plotted his data in a graph (Fig. 13) suggesting an exponential decay of erosion rates over time.

Nearly flat surfaces across original maar craters occur in two situations: First, when the ring rim is eroded but the crater is still filled with sediment, and second, when erosion has reached a level where the diatreme fill resists erosion as much as the country rock or where a weak fill is shielded from erosion by the country rock.

When the erosion level reaches resistant rocks in the diatreme, the maar evolves into a positive form (a hill) by relief inversion. Positive landforms can also occur in small

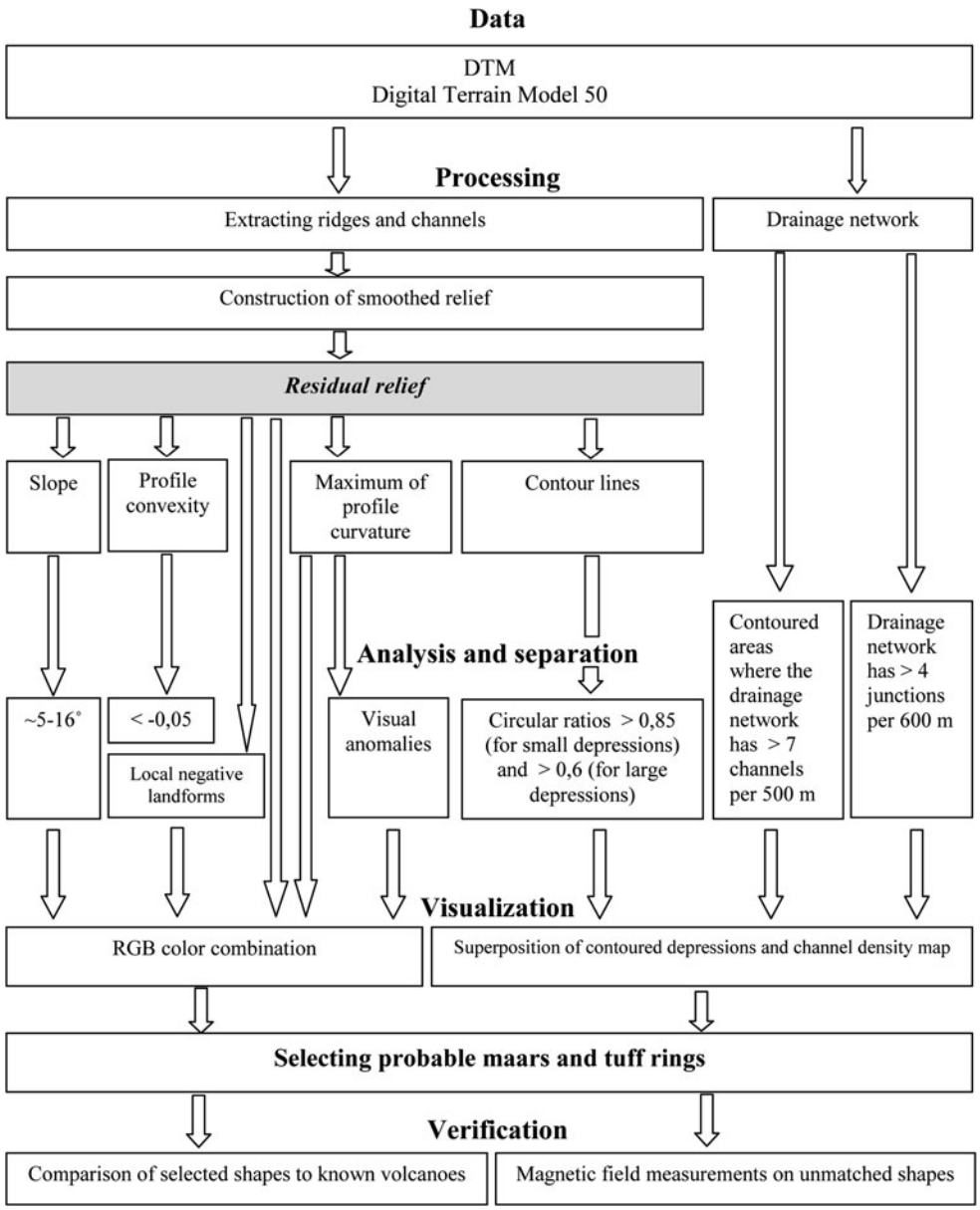

Fig. 7 Schematic outline of the work flow of this study

tuff rings or maars when landsliding from the inner slope of the tephra rim has created relief on the crater floor (e.g., in the Burlich and SE Bolsdorf tuff rings). However, positive morphological features can also be formed at an early stage before erosion reaches the diatreme. This happens if the surrounding rocks are less resistant to erosion than the rocks filling the crater. An example is the Waipiata Volcanic Field in New Zealand (Németh 2001), where the surrounding, poorly consolidated sedimentary rocks are softer than the pyroclastic rocks of the maar-diatremes. Most likely the formation of residual maar forms will evolve along a different path there and depend on the ratio of erodibility of host rocks to erupted rocks. The method outlined in the present paper would have to be adapted to such a scenario, but some search criteria would be the same, such as isometric shapes, ring structures and ring-shaped knicklines. In the West Eifel Volcanic Field, all stages of erosion can be observed, from young maars which have suffered very little erosion to those where the feeder pipe forms a hill.

Hesse (2000) reconstructed the Geeser Maar. His cross-sections of the original crater rim suggest maximum erosion of 170 m. Assuming that the Geeser Maar formed c. 100–200 ka ago (Hesse 2000), the erosion rate would be 0.85–1.7 mm per year. This is near the upper limit of the erosion rates estimated for similar areas. Burbank and Anderson (2001) describe a relationship of slope angles and ages of landforms. They show that slopes steeper than

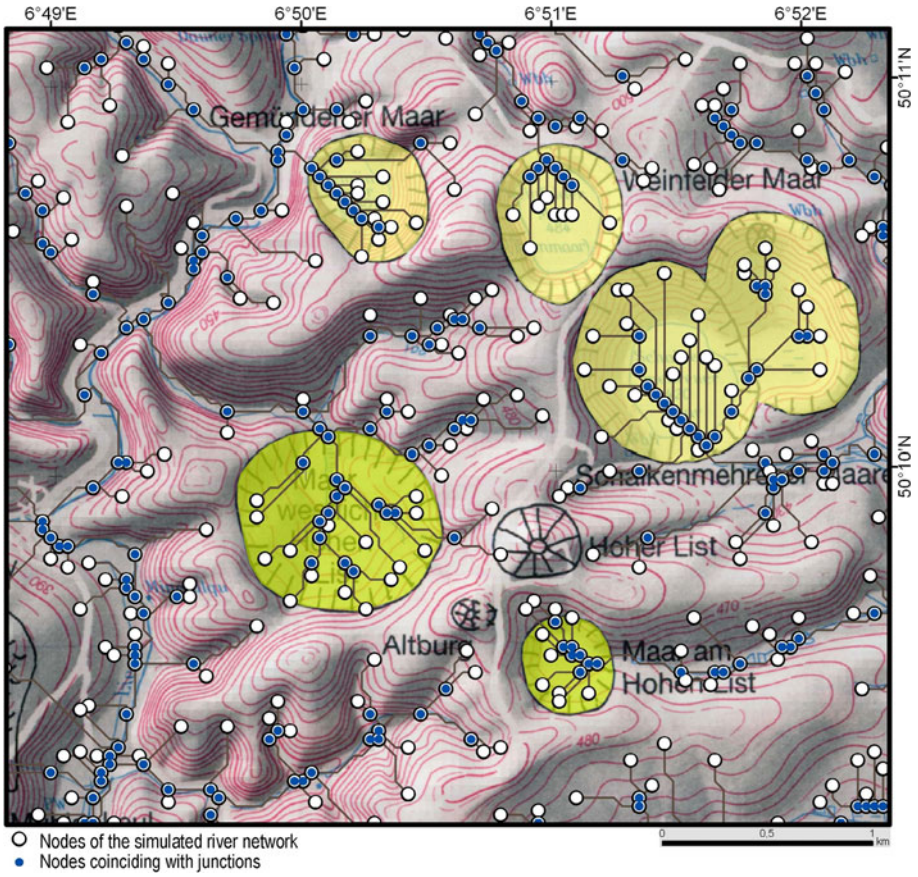

Fig. 8 River network simulated from the DTM. The mapped river network is also shown for comparison. In the simulated network, parallel channels stand out as artefacts on the maar crater floors. In the calculation of channel junction density, only nodes corresponding to junctions (*blue*) were used, whereas nodes representing channel start points or end points (*white*) were discarded. Maars of Group III are best accentuated by junction density (e.g. Aueler Maar Fig. 10e, Geeser Maar Fig. 10c). Tuff rings have often lost their initial ring shape (e.g. Gyppenberger Tuffring, Fig. 10b). Group IV is well represented (Fig. 10g, h). The shape of the Rother Maar (Fig. 10h) should probably be retraced following the outline of the anomaly. Figure 10a, b, f shows a good correspondence between junction density anomalies and nine maars verified through magnetic measurements on the ground

30° are consistent with tectonics younger than 10^3 years. The V-shaped cross profile of the river that dissected the Geeser Maar and valley flanks as steep as 31° suggests tectonic activity in the area which is younger than the Geeser Maar.

Despite its higher age, the Döttinger Maar preserves a more complete succession of lake sediments, suggesting no more than 200 m of erosion during 390 ka. This corresponds to an erosion rate of less than c. 0.5 mm per year. Close to the Döttinger Maar, there are Tertiary diatremes (Büchel 1994), with estimated ages between 44 and 35 Ma (Fekiacova et al. 2007). If these represent the roots of maars as proposed by (Mertes 1983; Büchel 1992; Fekiacova et al. 2007), and assuming an original maximum depth of some 2,000 m for them, the erosion rates were as low as 0.045–0.06 mm per year. This is 10 times lower than the erosion rate for the Döttinger Maar and 20 times less than that for the Geeser Maar. It is surprising that the Eckfelder Maar despite its high age of 45 Ma still has a complete succession of lake sediments and a bowl-shaped topography (Pirrung et al. 2003). Even at the low end of the range of erosion rates derived from other maars it should be eroded to the level of the feeder pipe or completely destroyed. This leads us to assume that the Eckfelder Maar was covered by Oligocene to Miocene sediments and did not erode at all for an extended period of time. In the NE part of the area studied, there occur intrusions and extrusions (Büchel 1994) which have been dated at 44–39 and 37–35 Ma (Ar/Ar) (Fekiacova et al. 2007) and interpreted as remains of volcanic structures similar to the Quaternary West Eifel volcanoes. Also in this case, there is no simple relationship between age and degree of erosion: the small intrusions interpreted as remnants of feeder pipes are younger than tuff pipes which should represent a shallower erosion level. It is likely that these Tertiary maars were also covered for some time but became exhumed earlier than the Eckfelder Maar. The strongly varying erosion states of old maars are thus indicative of differential uplift or subsidence and of different tectonic settings. The erosional history differs strongly with location, and short-term and long-term erosion rates can give clues to the local combination and succession of processes.

Fig. 9 Detail of the processed DTM data (Daun region). **a** Location ▶ of known maars on the residual relief surface, color-coded according to morphometric groups, **b** profile curvature raster, **c** contours of the residual relief, **d** density per area of channels, **e** contoured isometrically shaped depressions, **f** isometrically shaped areas of elevated junction density, **g** RGB color combination with R: profile convexity of the residual relief, G: slope of the residual relief and B: residual relief, **h** Superposition of **b**, **e**, and **f** in a single image

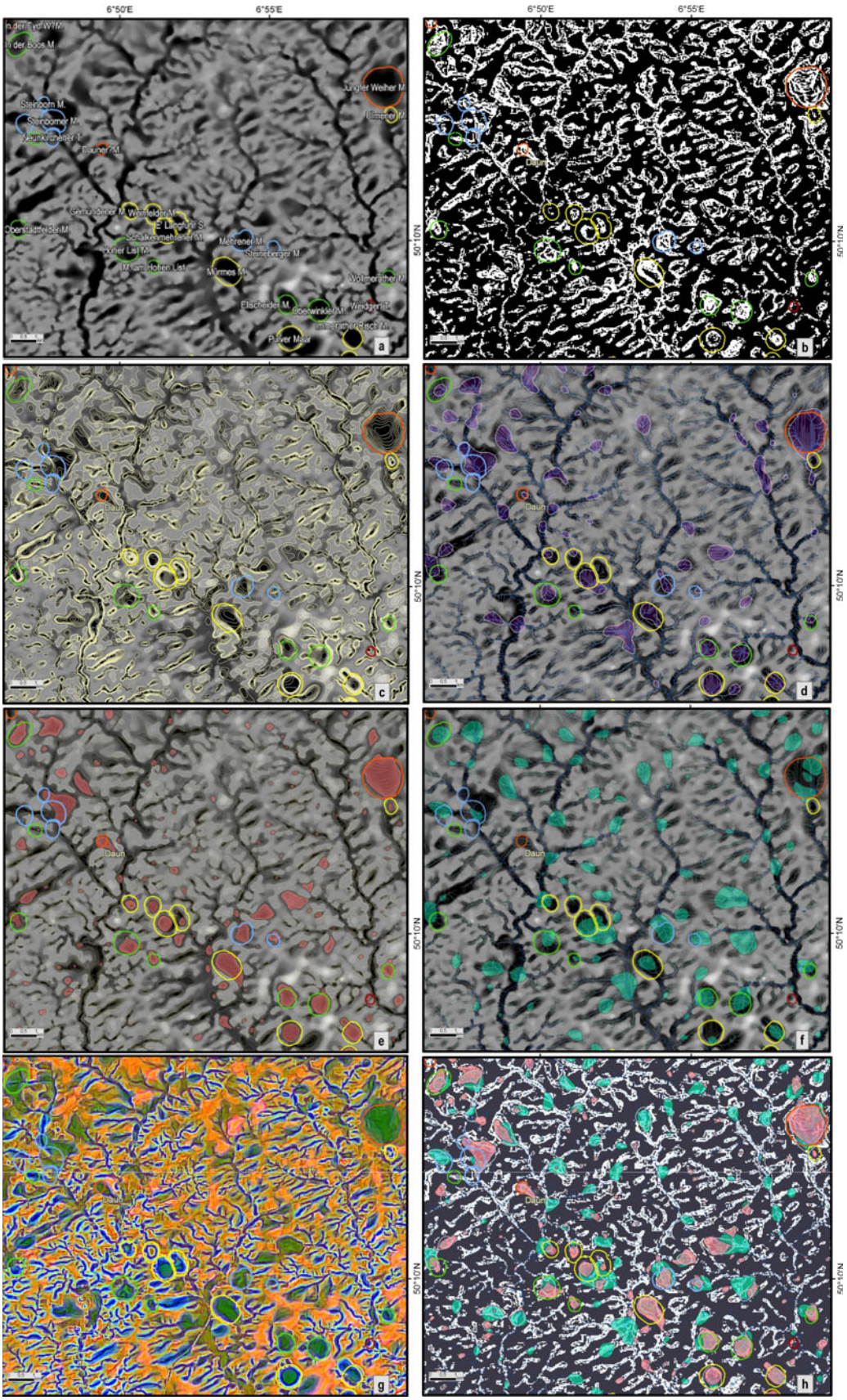
6°50'E
6°55'E
50°10'N
Daun
a
b
c
d
e
f
g
h

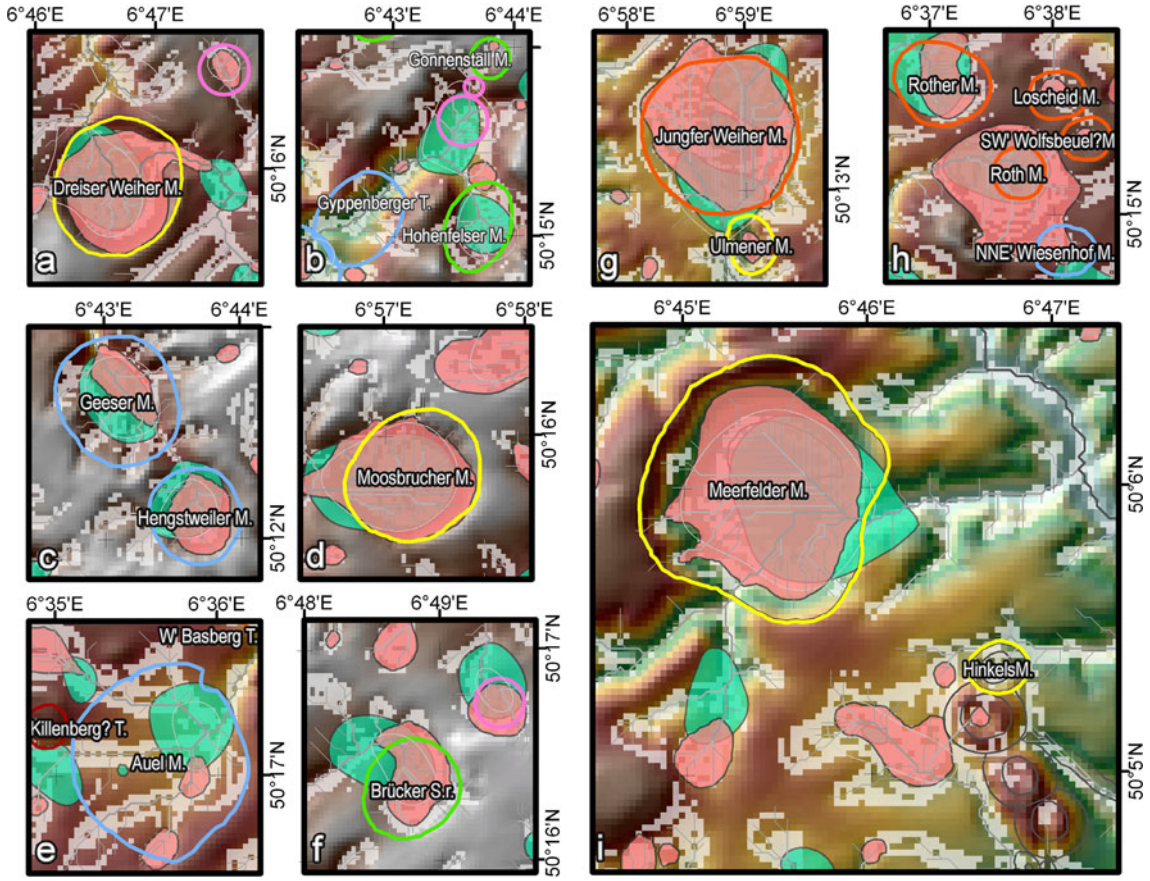

Fig. 10 Detail of known maars compared to accentuated topographic anomalies. Almost all maars from Groups I and II are highlighted through several criteria. Only a few maars which are either very small or non-isometric due to interference with other maars (Hohenfelser Maar, Fig. 10b) were not selected

Ages for the West Eifel Volcanic Field maars were published by several authors (Straka 1975; Büchel and Lorenz 1982; Büchel 1993; Mertes 1983; Meyer 1994; Zolitschka and Negendank 1995; Schmincke 2004; Schaber and Sirocko 2005). Many maars have not been dated yet. As of today, only 44 out of 95 maars are dated. Available ages are based on palynology and different isotopic dating methods (K/Ar, Ar/Ar, ^{14}C) and often vary strongly for the same maars depending on methods used and authors.

Our statistical analysis of maar age versus morphology is primarily based on the compilation by Schaber and Sirocko (2005; Table 5 in their paper). We preferentially used their recent ages derived from ^{14}C dating on sediment cores. In addition, we used some age data from other authors (Meyer 1994; Pirrung et al. 2003; Nowell et al. 2006) (Table 2). The minimum ages were taken as a first-order estimate of the maars' true ages. The West Eifel Volcanic Field maars formed at different times. The oldest one is the Eckfelder Maar, dated at 44 Ma. The next oldest maar-shaped volcano is the Hohenfelser Maar (660 ± 80 ka), followed by the W′(West) Basberg Maar (524 ± 197 ka). Five maars are bracketed between 345 and 460 and five maars between 130 and 140 ka, and two between 66 and 60 ka. From 45 ka through 7 ka, maar eruptions occurred at a relatively regular rate of 1–3 per 1 ka, with a maximum pause of 4 ka duration. The distribution of ages in the morphological groups (Fig. 5b) shows that ages for similarly eroded volcanoes scatter broadly. This points to strongly varying rates of erosion in the West Eifel Volcanic Field.

Most of the maars with ages younger than 45 ka are located east of the Eifel North–South depression. 30 out of 40 ages are younger than 45 ka. It is not clear whether this represents an actual increase in the frequency of maar eruptions or a better preservation of maar-diatreme volcanoes. The sampling of maars for age dating was probably biased toward the younger, better preserved structures, whereas strongly eroded or covered maars may be underrepresented.

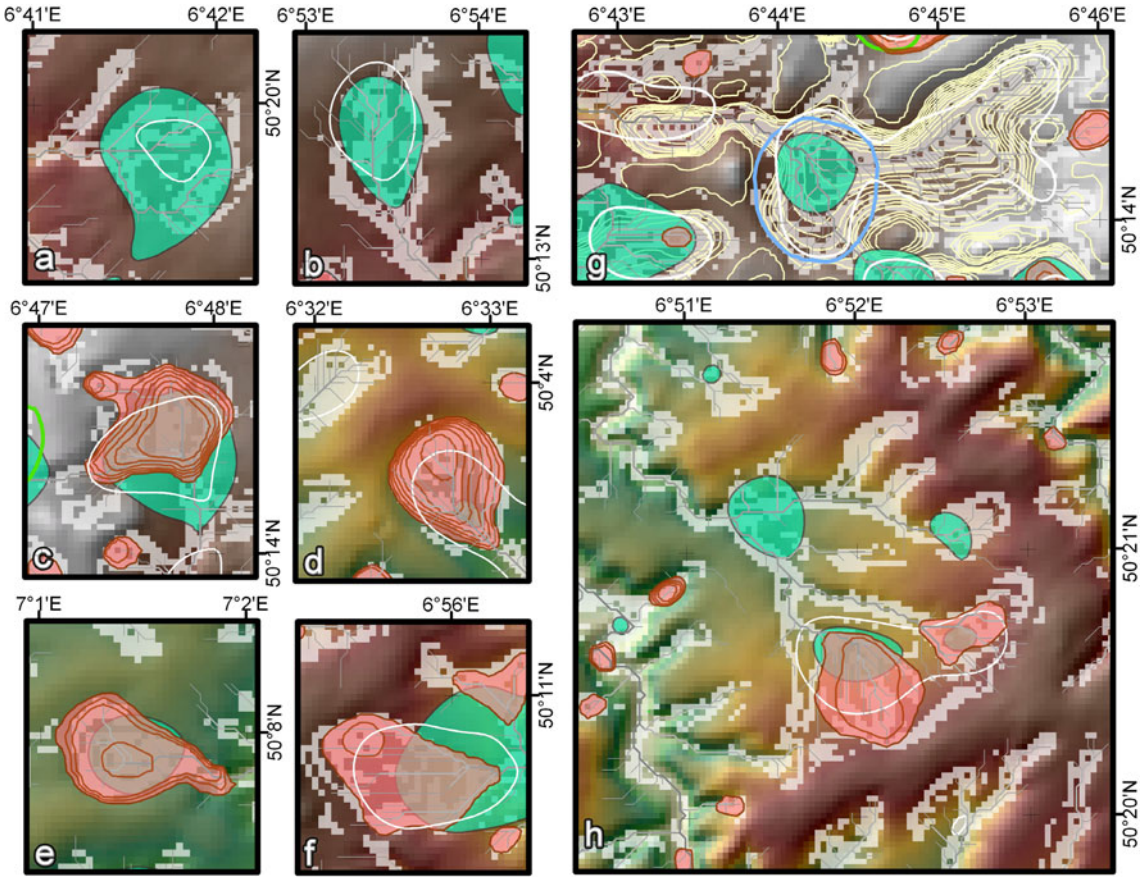

Fig. 11 Enlarged representation of some structures selected on the basis of associated anomalies resembling those of known maars. All of them exhibit characteristic patterns in the concavity raster and channel junction geometries. **c–e**, and **h** Show clear isometric contours in the residual relief (*red lines*), whereas **a**, **b** and **g** only show junction density anomalies. **g** shows an area of high junction density which is probably anisometric due to the overlapping of two or more maars. **h** shows a major annular structure coinciding with a depression and bifurcating 4th order channels. **e** is the only example with no increased channel density

Conclusions

On the basis of DTM data, we subdivided all known maars and similar volcanoes (tuff rings and "scoria rings") of the West Eifel Volcanic Field into five morphologic groups. We extracted and statistically analyzed the morphologic characteristics of known maars in the region in order to define criteria for the mapping of maars from DTMs and develop suitable workflows. The calculation of a residual relief surface as the difference between the original and smoothed land surfaces is particularly useful in aiding the identification of local anomalies. In the present study, we propose a method for regulating the tolerance of smoothing and the residual relief. The processed DTM data revealed not only the maars presently mapped but also structures with similar characteristics.

The preservation of maar shapes is not linearly dependent on age. This probably reflects a complex combination of parameters such as preexisting relief, river network evolution, and uplift rates varying in space and time. Erosion rates can thus only be estimated locally and cannot be extrapolated to adjacent areas. Age estimates should never be made based on preservation state alone. Estimates of erosion levels should not be based solely on preserved shapes but also take into account additional geologic information, such as the occurrence of xenoliths from (originally) overlying strata. For instance, Hanson (2007) gives an estimate for the erosion of kimberlites of South Africa based on the occurrence of xenoliths of upper Karoo basalt in the kimberlite pipes.

The spatial distribution of the erosion groups of the maars shows systematic differences between areas west and east of the N–S Eifel depression. The more strongly eroded maars tend to occur in the west, suggesting a higher uplift rate west of the N–S depression present-day.

Complex analysis of elevation data to reveal bowl-shaped features can not only be used for the identification of volcanic structures but also for other mapping tasks. More generally, the methods presented here can be adapted to any analysis or reconstruction of regional and local relief

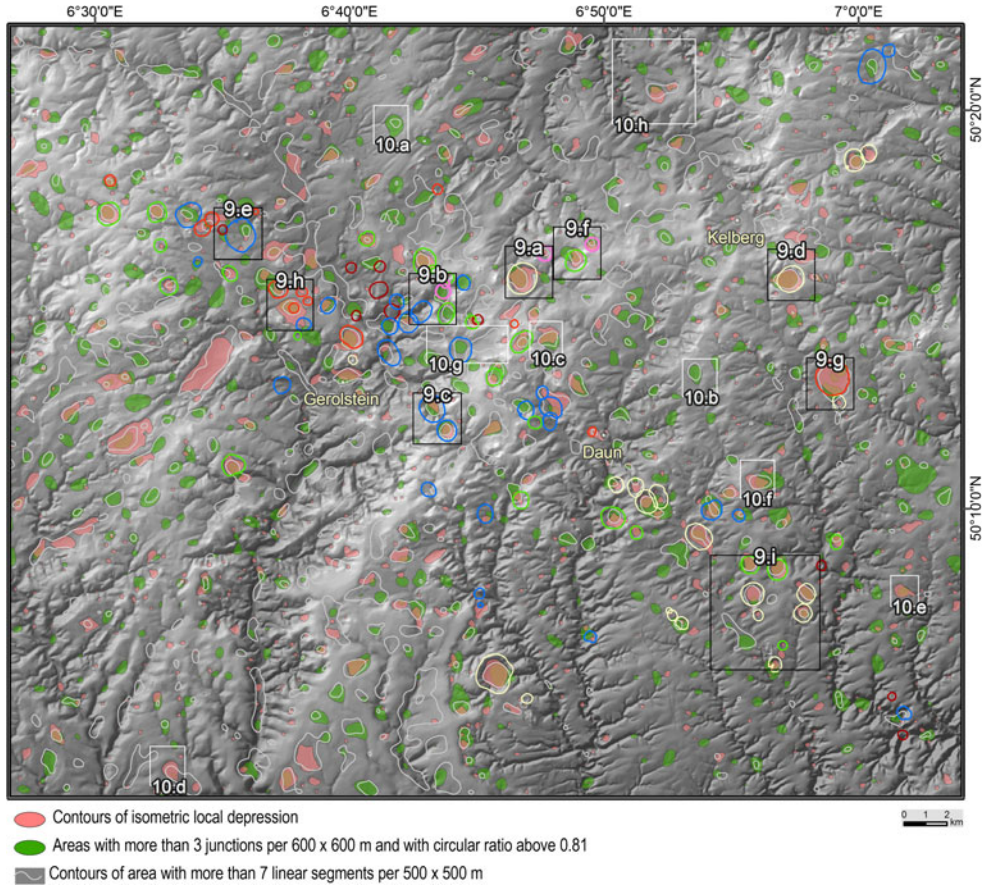

Fig. 12 Location of detected anomalies in the investigated area

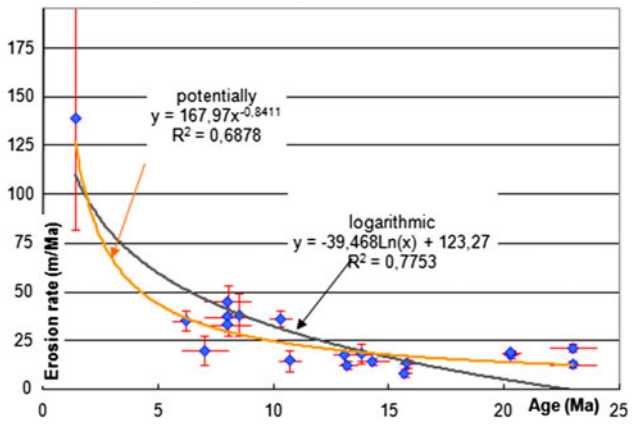

Fig. 13 Erosion rates as a function of age for maars of the French Massif Central (data from Degeai 2004). Erosion rates decrease with age. A drop in erosion rate occurs as soon as the tuff rim has been eroded

as a basis for (semi)-quantitative studies of geomorphologic processes. The methods can also be used in the analysis of micro-surfaces, such as vesicular or granular structure, and can be adapted to local changes.

Acknowledgments We thank Jutta Winsemann and Ulrich Asprion (Hannover) and Lothar Ratschbacher (Freiberg) for helpful discussions and suggestions and for the possibility to work on this paper. Mathias Leidig and Richard Gloaguen (Freiberg) helped with all kinds of computer problems. Michael Pirrung read an earlier version of the manuscript and gave us many helpful hints. We are also grateful to Peter Frenzel for his feedback and adjustments. Many thanks to Károly Németh for his detailed and thoughtful review and to editor-in-chief Wolf-Christian Dullo for his assistance. They all helped us to substantially improve the paper.

References

Beget JE, Hopkins DM, Charron SD (1995) The largest maars on Earth, Seward Peninsula, northwest Alaska. Arctic 49:62–69

Büchel G (1987) Geophysik der Eifelmaare. 1: Erkundung neuer Maare im Vulkanfeld der Eifel mit Hilfe geomagnetischer Untersuchungen. Mainzer geowiss Mitt 16:227–274, 36 Abb.; Mainz

Büchel G (1992) Das Kelberger Hoch. Tiefenstruktur und Geodynamik einer magnetischen Anomalie in der Eifel. Die Geowissenschaften 5:132–142

Büchel G (1993) Maars of the Westeifel, Germany. In: Negendank JFW, Zolitschka B (eds) Paleolimnology of European maar lakes. Lecture notes in earth sciences, vol 49. Springer, Berlin, pp 1–13

Büchel G (1994) Vulkanologische Karte der West- und Hocheifel 1:50.000, Koblenz (Landesvermessungsamt Rheinland-Pfalz)

Büchel G, Lorenz V (1982) Zum Alter des Maarvulkanismus der Westeifel (The age of the West Eifel Maar volcanism). Neues Jahrbuch für Geologie und Paläontologie 163(1):1–22

Büchel G, Mertes H (1982) Die Eruptionszentren des Westeifeler Vulkanfeldes (The eruption centers of the West Eifel Volcanic Field). Zeitschrift der Deutschen Gesellschaft Geowissenschaften 133:409–429

Büchel G, Pirrung M (1993) Tertiary maars of the Hocheifel Volcanic Field, Germany. In: Negendank JWF, Zolitschka B (eds) Lecture notes in earth sciences. Paleolimnology of European Maar Lakes, vol 49. Springer, Berlin, pp 447–465

Bundesanstalt für Geowissenschaften und Rohstoffe (2003) Bearbeitungsstand. Digitale Geowissenschaftliche Karte der Bundesrepublik Deutschland. Grundlage: Geologische Karte der Bundesrepublik Deutschland 1:1 000 000 von Voges A et al (1993) Hannover

Burbank DW, Anderson RS (2001) Tectonic geomorphology. Blackwell Science, Oxford, p 274

Cas RAF, Hayman P, Pittari A, Porritt L (2008) Some major problems with existing models and terminology associated with kimberlite pipes from a volcanological perspective, and some suggestions. J Volcanol Geotherm Res 174:209–225

Degeai J-P (2004) Mesure de l'érosion post-éruptive autour des cratères de maars en inversion de relief dans le Massif Central français./Post-eruptive erosion measurement around the inverted maar craters in the French Massif Central. Géomorphologie: relief, processus, environnement 4:285–304

Evans IS (1979) An integrated system of terrain analysis and slope mapping. Final report on grant DA-ERO-591-73-G0040, University of Durham, England

Fekiacova ZD, Mertz F, Renne PR (2007) Geodynamic setting of the Tertiary Hocheifel volcanism (Germany), Part I: $^{40}Ar/^{39}Ar$ geochronology. In: Ritter JRR, Christensen UR (eds) Mantle Plumes—a multidisciplinary approach. Springer, Heidelberg, pp 185–206

Franz G, Breitkreuz C, Coyle DA, El Hur B, Heinrich W, Paulick H, Pudlo D, Smith R, Steiner G (1997) The alkaline Meidob volcanic field (Late Cenozoic, northwest Sudan). J Afr Earth Sci 25:263–291

Garcia-Castellanos D, Cloetingh S, Van Balen R (2000) Modelling the Middle Pleistocene uplift in the Ardennes-Rhenish Massif: thermo-mechanical weakening under the Eifel? Glob Planet Change 27(1–4):39–52

Garcin Y, Williamson D, Taieb M, Vincens A, Mathe PE, Majule A (2006) Centennial to millennial changes in maar-lake deposition during the last 45.000 years in tropical Southern Africa (Lake Masoko, Tanzania). Palaeogeogr Palaeoclimatol Palaeoecol 239:334–354

Grohmann C, Riccomini C, Alves F (2007) SRTM-based morphotectonic analysis of the Poços de Caldas Alkaline Massif, southeastern Brazil. Comput Geosci 33(1):10–19

Hanson EK (2007) Estimating erosion of Cretaceous-aged kimberlites in the Republic of South Africa through the examination of upper-crustal xenoliths. Unpublished MSc thesis, Rhodes University, South Africa, p 138

Hesse G (2000) Hydrogeologische Erkundung von Maar-Diatrem-Vulkanen am Beispiel des Geeser Maares (Westeifel). Unpublished PhD thesis, Friedrich-Schiller Universität Jena, p 135

Huckenholz HG, Büchel G (1988) Tertiärer Vulkanismus der Hocheifel. Fortschr Miner 66(2):43–82

Illies H, Prodehl C, Schmincke HU, Semmel A (1979) The quaternary uplift of the rhenish shield in Germany. Tectonophysics 61: 197–225

Kamenetsky MB, Sobolev AV, Kamenetsky VS, Maas R, Danyushevsky LV, Thomas R, Pokhilenko NP, Sobolev NV (2004) Kimberlite melts rich in alkali chlorides and carbonates: a potent metasomatic agent in the mantle. Geology 32:845–848

Lorenz V (1973) On the formation of maars. Bull Volcanol 37(2):138–204

Lorenz V (1975) Formation of phreatomagmatic maar-diatreme volcanoes and its relevance to kimberlite diatremes. Phys Chem Earth 9:17–27

Lorenz V (1986) On the growth of maars and diatremes and its relevance to the formation of tuff-rings. Bull Volcanol 48:265–274

Lorenz V (2003) Maar-diatreme volcanoes, their formation, and their setting in hard-rock or soft-rock environments. GeoLines J Geol Inst AS Czech Repub 15:72–83

Lorenz V (2007) Syn- and posteruptive hazards of maar-diatreme volcanoes. J Volcanol Geotherm Res 159(1–3):285–312

Lorenz V, Büchel G (1980) Die Kesseltäler der vulkanischen Westeifel; Nachweis ihrer Maargenese. Mainzer Geowiss Mitt 8:173–191

Lorenz V, Kurszlaukis S (2007) Root zone processes in the phreatomagmatic pipe emplacement model and consequences for the evolution of maar-diatreme volcanoes. J Volcanol Geotherm Res 159:4–32

Lustrino M, Carminati E (2007) Phantom plumes in Europe and neighbouring areas: In: Foulger GR, Jurdy DM (eds) Plates, plumes, and planetary processes. Geol. Soc. Am. Spec. paper 430, pp 723–746

Martin U, Németh K, Lorenz V, White JDL (2007) Introduction: Maar-diatreme volcanism. J Volcanol Geotherm Res 159(1–3): 1–3. doi:10.1016/j.jvolgeores.2006.06.003

Martín-Serrano A, Vegas J, García-Cortés A, Galán L, Gallardo-Millán JL, Martín-Alfageme S, Rubio FM, Ibarra PI, Granda A, Pérez-González A, García-Lobón JL (2009) Morphotectonic setting of maar lakes in the Campo de Calatrava Volcanic Field (Central Spain, SW Europe). Sediment Geol 222:52–63

May F (2005) Alteration of wall rocks by CO_2-rich water ascending in fault zones: natural analogues for reactions induced by CO_2 migrating along faults in siliciclastic reservoir and cap rocks. Oil Gas Sci Technol. Rev IFP 60(1):19–32. doi:10.2516/ogst:2005003

May F, Hoernes S, Neugebauer H (1996) Genesis and distribution of mineral waters as a consequence of recent lithospheric dynamics: the Rhenish Massif, Central Europe. Geol Rundsch 85:782–799

Mertes H (1983) Aufbau und Genese des Westeifeler Vulkanfeldes. Bochum Geol u Geotechn Arb Bochum 9:1–415

Mertes H, Schmincke H-U (1985) Mafic potassic lavas of the Quaternary West Eifel Volcanic Field. I. Major and trace elements. Contrib Mineral Petrol 89:330–345

Meyer W (1994) Geologie der Eifel. 3. Aufl. Schweizerbart′sche Verlagsbuchhandlung, Stuttgart, p 615

Meyer W, Stets J (2002) Pleistocene to recent tectonics in the Rhenish Massif (Germany). Neth J Geosci/Geologie en Mijnbouw 81: 217–221

Moss S, Russell JK, Andrews GDM (2008) Spatio-temporal evolution of kimberlite magmas at Diavik, NWT. In: 9th International Kimberlite conference. Extended abstract 9IKC-A-00302

Németh K (2001) Long-term erosion-rate calculation from the Waipiata Volcanic Field (New Zealand) based on erosion remnants of scoria cones, tuff rings and maars. Géomorphologie: relief, processus, environnement (Paris-Lyon) 2:137–152

Németh K (2003) Calculation of long-term erosion in Central Otago, New Zealand, based on erosional remnants of maar/tuff rings. Zeitschrift für Geomorphologie NF 47:29–49

Németh K, Cronin SJ (2007) Syn- and post-eruptive erosion, gully formation, and morphological evolution of a tephra ring in tropical climate erupted in 1913 in West Ambrym, Vanuatu. Geomorphology 86:115–130

Németh K, Martin U (1999) Late Miocene paleo-geomorphology of the Bakony-Balaton Highland Volcanic Field (Hungary) using physical volcanology data. Zeitschrift für Geomorphologie 43:417–438

Németh K, White JDL (2003a) Geochemical evolution, vent structures, and erosion history of small-volume volcanoes in the Miocene Intracontinental Waipiata Volcanic Field, New Zealand. Geolines J AS Czech Repub (Proceedings for the Hibsch 2002 Prague meeting on "Alkaline basaltic continental rift related magmatism") 15:63–69

Németh K, White JDL (2003b) Reconstructing eruption processes of a Miocene monogenetic volcanic field from vent remnants: Waipiata Volcanic Field, South Island, New Zealand. J Volcanol Geotherm Res 124:1–21

Németh K, Martin U, Csillag G (2003) Calculation of erosion rates based on remnants of monogenetic alkaline basaltic volcanoes in the Bakony-Balaton Highland Volcanic Field (Western Hungary) of Mio/Pliocene age. Geolines 15:93–97

Nowell DAG, Jones MC, Pyle DM (2006) Episodic Quaternary volcanism in France and Germany. J Quat Sci 21(6):645–675

Pirrung M, Fischer C, Büchel G, Gaupp R, Lutz H, Neuffer F-O (2003) Lithofacies succession of maar crater deposits in the Eifel area (Germany). Terra Nova 15:125–132

Pirrung M, Büchel G, Lorenz V, Treutler H (2008) Post-eruptive development of the Ukinrek East Maar since its eruption in 1977 A.D. in the periglacial area of south-west Alaska. Sedimentology 55(2):305–334

Roberts A (2001) Curvature attributes and their interpretation to 3D interpreted horizons. First Break 19:85–100

Ross P-S, Delpit S, Haller MJ, Németh K, Corbella H (2010) Influence of the substrate on maar-diatreme volcanoes—an example of a mixed setting from the Pali Aike volcanic field, Argentina. J Volcanol Geotherm Res 20(1–4):253–271

Russell JK, Moss S (2006) Volatiles and kimberlite eruption: insights from Diavik. Kimberlite emplacement workshop, long abstract, p 5

Schaber K, Sirocko F (2005) Lithologie und Stratigraphie der spätpleistozänen Trockenmaare der Eifel. Mainzer Geowiss Mitt 33:295–340

Schäfer A, Utescher T, Klett M, Valdivia-Manchego M (2005) The Cenozoic Lower Rhine Basin—rifting, sedimentation, and cyclic stratigraphy. Int J Earth Sci 94:621–639

Schmincke H-U (2004) Volcanism. Springer, Heidelberg, pp 1–324

Schmincke H-U (2007) The Quaternary Volcanic Fields of the East and West Eifel (Germany). In: Ritter JRR, CUR (eds) Mantle Plumes—a multidisciplinary approach. Springer, Berlin, pp 241–322. doi:10.1007/978-3-540-68046-8_8

Schmincke H-U (2010) Vulkanismus (Volcanism). Wissenschaftliche Buchgesellschaft, Darmstadt. ISBN 978-3-534-23628-2

Schulz R, Buness H, Gabriel G, Pucher R, Rolf C, Widerhold H, Wonik T (2005) Detailed investigation of preserved maar structures by combined geophysical surveys. Bull Volcanol 68:95–106. doi:10.1007/s00445-005-0424-8

Seib N, Kley J, Torizin E, Zander I, Goepel A, Büchel G (2008) Identifikation vulkanischer Formen in einem digitalen Geländemodell (DGM) der Westeifel (Identification of volcanic landforms in a Digital Terrain Model (DTM) of the Westeifel). Zeitschrift der Deutschen Gesellschaft Geowissenschaften 159(4):657–670

Shaw CSJ, Eyzaguirre J, Fryer B, Gagnon J (2005) Regional variations in the mineralogy of metasomatic assemblages in mantle xenoliths from the West Eifel Volcanic Field, Germany. J Petrol 46:945–972

Smith BHS, Berryman AK (2007) Reply to discussion of "Geology and diamond distribution of the 140/141 kimberlite, Fort a la Corne, central Saskatchewan, Canada" by Berryman AK, Scott Smith BH and Jellicoe BC Lithos 76:99–114, by Kjarsgaard BA, Leckie DA and Zonneveld JP. Lithos 97:429–434

Sorohtin OG (1985) Tectonica litosphernyh plit i proishojdenie almasonosnyh kimberlitov (Tectonic of the lithospheric plates and origin of diamonds kimberlites) Obschaia i regionalnaia geologia; geologicheskoe kartirovanie, p 48, (in Russian) Moscow. MG USSR, AWUSSR

Sorohtin OG, Ushakov SA (2002) Development of the Earth. Moscow University, Moscow, p 506 (in Russian). http://macroevolution.narod.ru/sorohtin.htm

Stachel T, Büchel G (1989) Das Döttinger Maar: Fallstudie eines großen tertiären (?) Tuffschlotes im Vulkanfeld der Hocheifel. (The Döttingen Maar: Case study of a large Tertiary (?) diatreme of the Hocheifel Volcanic Field.). Zeitschrift der Deutschen Gesellschaft Geowissenschaften 140:35–51

Strahler AN (1952) Hypsometric (area-altitude) analysis of erosional topology. Geol Soc Am Bull 63(11):1117–1142. doi:10.1130/0016-7606(1952)63[1117:HAAOET]2.0.CO;2

Strahler AN (1957) Quantitative analysis of watershed geomorphology. Trans Am Geophys Union 8(6):913–920

Straka H (1975) Die spätquartäre Vegetationsgeschichte der Vulkaneifel. Pollenanalytische Untersuchungen an vermoorten Maaren. (The late Quaternary vegetation history of the volcanic Eifel. Pollen analyses of marshy maars). In: Landesamt für Umweltschutz Rheinland-Pfalz (ed) Beiträge zur Landespflege in Rheinland Pfalz. 3, Oppenheim, p 163

Suhr P, Goth K, Lorenz V, Suhr S (2006) Long lasting subsidence and deformation in and above maar-diatreme volcanoes a never ending story. Zeitschrift der Deutschen Gesellschaft Geowissenschaften 157(3):491–511

Viereck L (1984) Geologische und petrologische Entwicklung des pleistozänen Vulkankomplexes Rieden, Ost-Eifel. Bochumer Geol Geotechn Arb 17:1–337

Walters AL, Phillips JC, Brown RJ, Field M, Gernon T, Stripp G, Sparks RSJ (2006) The role of fluidisation in the formation of volcaniclastic kimberlite: grain size observations and experimental investigation. J Volcanol Geotherm Res 1–2:119–137

White JDL, Ross PS (2011) Maar-diatreme volcanoes: a review. J Volcanol Geotherm Res 201:1–29

Wilson M, Downes H (1991) Tertiary-Quaternary extension related alkaline magmatism in western and central Europe. J Petrol 32:811–849

Wilson L, Head JW (2007) An integrated model of kimberlite ascent and eruption. Nature 47(7140):53–57. doi:10.1038/nature05692

Wood CA (1974) Reconnaissance geophysics and geology of Pinacate Craters, Sonora, Mexico. Bull Volcanol 38:149–172

Wood JD (1996) The geomorphological characterisation of digital elevation models. PhD thesis, University of Leicester, UK. http://www.soi.city.ac.uk/~jwo/phd, http://sideshow.jpl.nasa.gov/mbh/series.html

Ziegler PA, Dèzes P (2007) Cenozoic uplift of Variscan Massifs in the Alpine foreland: timing and controlling mechanisms. Glob Planet Change 58(1–4):237–269

Zolitschka B, Lottermoser JFW, Negendank Lottermoser BG (1995) Sedimentological proof and dating of the Early Holocene volcanic eruption of Ulmener Maar (Vulkaneifel, Germany). Geol Rundsch 84(1):213–219

Zăvoianu I (1985) Morphometry of drainage basins/Ion Zăvoianu; [translated from the Romanian by Adriana Ionescu-Pârâu]. Elsevier, p 238. ISBNs: 0444995870, 9780444995872